J Mol Model (2009) 15:1517–1539
DOI 10.1007/s00894-009-0511-4

ORIGINAL PAPER

A 3-D model of tumor progression based on complex automata driven by particle dynamics

Rafał Wcisło · Witold Dzwinel · David A. Yuen · Arkadiusz Z. Dudek

Received: 2 February 2009 / Accepted: 20 March 2009 / Published online: 23 May 2009

Abstract The dynamics of a growing tumor involving mechanical remodeling of healthy tissue and vasculature is neglected in most of the existing tumor models. This is due to the lack of efficient computational framework allowing for simulation of mechanical interactions. Meanwhile, just these interactions trigger critical changes in tumor growth dynamics and are responsible for its volumetric and directional progression. We describe here a novel 3-D model of tumor growth, which combines particle dynamics with cellular automata concept. The particles represent both tissue cells and fragments of the vascular network. They interact with their closest neighbors *via* semi-harmonic central forces simulating mechanical resistance of the cell walls. The particle dynamics is governed by both the Newtonian laws of motion and the cellular automata rules. These rules can represent cell life-cycle and other biological interactions involving smaller spatio-temporal scales. We show that our complex automata, particle based model can reproduce realistic 3-D dynamics of the entire system consisting of the tumor, normal tissue cells, blood vessels and blood flow. It can explain phenomena such as the inward cell motion in avascular tumor, stabilization of tumor growth by the external pressure, tumor vascularization due to the process of angiogenesis, trapping of healthy cells by invading tumor, and influence of external (boundary) conditions on the direction of tumor progression. We conclude that the particle model can serve as a general framework for designing advanced multiscale models of tumor dynamics and it is very competitive to the modeling approaches presented before.

Keywords Angiogenesis · Complex automata · Computer simulation · Discrete particle model · Tumor progression

R. Wcisło · W. Dzwinel (✉)
Institute of Computer Science,
AGH University of Science and Technology,
Al. Mickiewicza 30,
30-059 Krakow, Poland
e-mail: dzwinel@agh.edu.pl

R. Wcisło
e-mail: wcislo@agh.edu.pl

D. A. Yuen
Minnesota Supercomputing Institute, University of Minnesota,
Minneapolis, MN 55455-0219, USA
e-mail: daveyuen@gmail.com

A. Z. Dudek
Division of Hematology, Oncology, and Transplantation,
Department of Medicine,
University of Minnesota Medical School,
Minneapolis, MN 55455-0219, USA
e-mail: dudek002@umn.edu

Introduction

Despite the huge amount of resources that have been devoted to cancer research, according to the National Center for Health Statistics (http://www.cdc.gov/nchs/FASTATS/lcod.htm), cancer is the second killer (after heart disease) in the US. The set of diseases, which are categorized as cancer, are characterized by serious disruptions in the control mechanisms regulating growth and homeostasis in normal tissue. Up to now many aspects of cancer remain obscure for experimentalists and clinicians, and many of the currently used therapeutic strategies are not entirely effective.

A better understanding of the dynamics of tumor formation and its growth are expected from computer models and simulations. The modeling could improve the overall clinical outcome by predicting the results of specific

forms of treatment administered at specific time points. Moreover, it might help to optimize the existing therapeutic procedures, design new ones, or even provide post-treatment predictions [1–4]. The degree of angiogenesis in human tumors varies widely and may be very low in some types of tumors. Therefore, tumors with a low level of angiogenesis may not be benefited when treated with antiangiogenic agents [2, 5]. Computer modeling of tumor progression involving its both avascular and vascular phases, could allow for answering the question if the angiogenic therapy is justified or not in these uncertain cases.

Nevertheless, we should be aware of the computer modeling limitations from which the most important are as follows:

1. The replication of living organism *in silico* is a computationally irreducible problem due to impassable barriers of the theory of computation, the theory of chaos and technological limits. Many aspects of tumor development can be investigated on a case-by-case basis.
2. Tumor evolution is a complex process involving processes occurring over a variety of time and length scales: from the DNA level and intracellular processes, through tumor vascularization and metastasis, to the holistic, mental and environmental factors. Up to now, no significant progress has been made in constructing consistent and rigorous mathematical formalism and computational methodologies, which can exploit efficiently current computational resources and programming paradigms in modeling truly multiscale phenomena.
3. Even well known physical processes occurring in the real tissue, such as diffusion and blood flow, which can be described using partial differential equations (PDEs), are very difficult to simulate. This is due to the intricate boundary conditions imposed by heterogeneous environment (e.g., extracellular matrix (ECM) structure, blood vessel structure, blood rheology *etc*.), incomplete parameter space, and non-linear reaction terms.

Although global modeling of cancer development is impossible, a more selective approach focusing on basic carcinogenic processes can allow for substantial reduction of both many methodological problems and computational resources. The approximate theories and numerical models can be used then to detect more precisely the cancer "weak points" - the future targets of anticancer therapeutic strategies.

We focus our attention on the process of tumor growth from avascular phase to angiogenic phase, i.e., the process of the blood vessel formation from a pre-existing vasculature. Judah Folkman published in 1971 the theory [6, 7] that angiogenesis is a principal process in tumor progression [9, 10]. Vascularized tumor invades the surrounding tissue, blood and lymphatic vascular systems and the possibility of the cancer spreading (metastasis) increases dramatically. Antiangiogenic targeting of the neovasculature within tumors is currently considered as one of the most promising strategies in the search for novel antineoplastic therapies [2, 6, 11]. Because molecular phenotype of immature, angiogenic blood vessels is distinctly different from that of resting blood vessels, tumor blood vessels can be selectively targeted without affecting the normal organ vasculature. The process of angiogenic signaling and formation of blood vessels can be disrupted or slowed down with small molecules. In addition to treatments directed to specific target, non specific agents can be used to eliminate endothelial cells thus inhibiting angiogenesis. This involves numerous expensive and demanding investigations both of hundreds of factors inhibiting angiogenesis and antiangiogenic chemical species which can be considered in drug design process. To cut expenses, the predictive power of mathematical modeling and computer simulation has to be employed. As shown in [12], *in silico* experiments can play the role of angiogenesis assays.

In the following section we shortly describe the main processes, phenomena and growth factors contributing cancerogenesis. Then we present the most advanced models of tumor growth including continuum, cellular automata and hybrid models. We focus on such modeling aspects as cell cycle, tumor growth factors, angiogenesis, blood flow, and vessel remodeling. Next, we describe the model of complex automata driven by particle dynamics and we discuss its assumptions, limitations, and simulation conditions. The following section collects the results from simulation of avascular and vascular phases of tumor growth. We scrutinize the role of mechanical interactions between swelling tumor, normal tissue, and expanding vascular network on tumor dynamics. We explain the influence of mechanical interactions on compartmentalization of the avascular tumor into external shell of well oxygenated cells, deeper layer of cells in hypoxia and necrotic interior. We study the effect of mechanical remodeling on tumor progression in vascular phase and on differentiation of microvascular density in various regions of tumor. The role of processes involved in branching and vessels maturation, such as (Dll4) - Noch1 signaling [13, 14], is also analyzed. The results are confronted with experimental studies. For simplicity we do not discuss a parallel to blood vessel, lymph vessel network which assist normal tissue and tumor with lymph outflow and decrease in extracellular matrix pressures. This network is a critical component of tumor metastases pathway. However, it is only minimally involved in dynamics of tumor growth. In the last section we present the conclusions.

Simplistic model of tumor growth

Generally, we can recognize a few principal phases of tumor progression, representing various spatio-temporal scales [1, 15–17].

1. Subcellular scale - involves genetic changes, distortion in the cell cycle and loss of apoptosis, absorption of vital nutrients.
2. Cellular scale - comprises interaction at the cellular level with immune cells and other tumor cells, activation and inhibition of the immune system. The cellular scale refers to the main activities of the cells: activation and proliferation of tumor cells.
3. Avascular tumor scale - includes condensation of tumor cells into cluster, macroscopic diffusion of TAF (tumor angiogenic factors) and oxygen.
4. Angiogenic phase - involves angiogenesis, sprouting, anastomosis, angiogenesis termination.
5. Vascular phase - includes blood flow, remodeling (vessel dilation and regression, mechanical reshaping of tumor and vessels), vessel maturation.
6. Detachment of metastases and invasion.

In Fig. 1 we present the scale separation map (SSM) for this simplified model of tumor growth. The microscopic processes such as cell motility and cell cycle are discrete. The macroscopic scale refers to phenomena which are typical for continuum systems such as diffusion (of oxygen and TAF), overall tumor condensation and blood flow. In macroscopic models, microscopic phases can be approximated by coarse grained models as long as the methodology of multi-scale simulation and adequate computational resources are lacking. The arrows in Fig. 1 show the relationships between these processes. The particle model presented in the following sections refers only to the processes shaded in blue.

Four overlapping phases of tumor growth are usually identified: the avascular phase, the angiogenic phase, the vascular phase, and vessels and tumor remodeling. These phases go with physical processes such as nutrients and TAF diffusion, blood flow and mechanical remodeling caused by interaction between growing tumor, vessels and the normal tissue.

Avascular tumor

The proliferating tumor cells start to condensate into a compact cluster and interact with the external environment. Solid tumor, which is smaller than 1–2 mm in diameter (about 10^6–10^7 cells [11]), removes wastes and acquires nutrients and oxygen through passive diffusion. The oxygen (and nutrients) is supplied to the tumor nucleus by the closest, mature blood vessels. It percolates through the surface of the solid tumor and diffuses inside its mass. Due

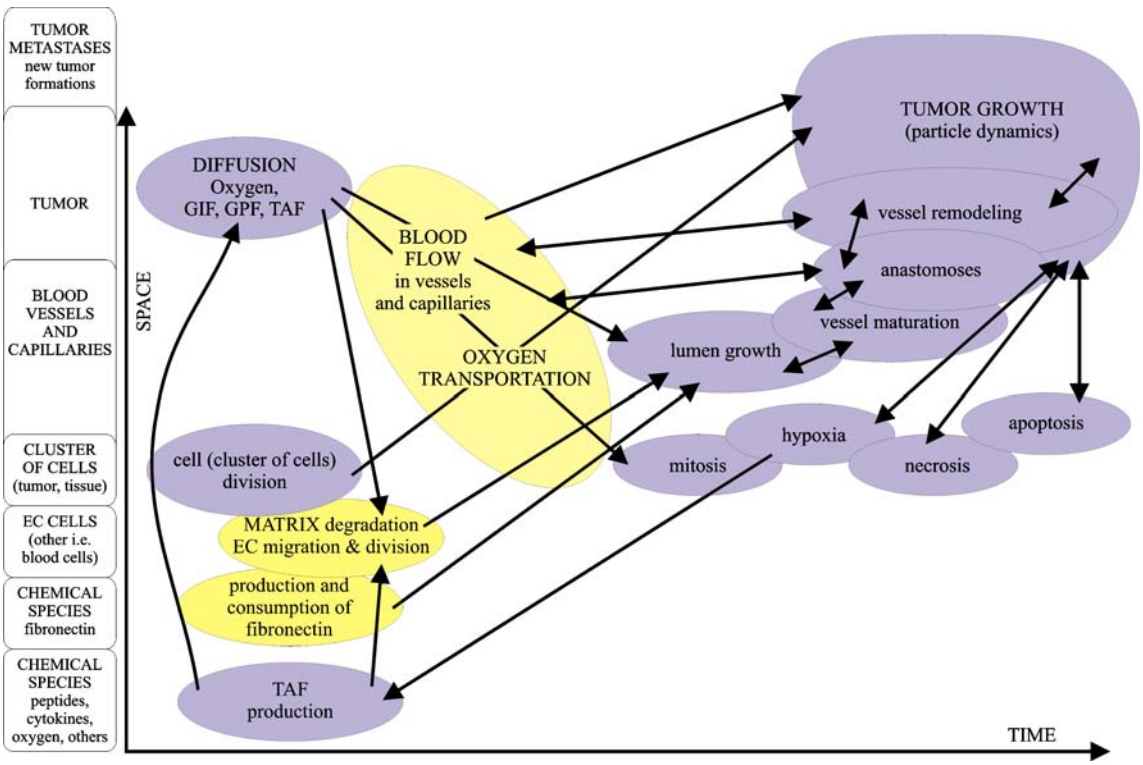

Fig. 1 The scale separation map of all the main processes considered in modeling of tumor-induced angiogenesis. The processes controlled in our model are colored blue

to differences in concentration of oxygen, the tumor cluster consists of the outer region with proliferating cells, an intermediate region of cells in hypoxia and the necrotic core of dead tumor cells. Most solid tumors, even those 1–3 mm in diameter, exhibit hypoxic fractions that may range from 10 to 30% [11, 18, 19]. The avascular tumor is in dynamic equilibrium. Its critical mass has been reached, and diffusion based transport is no longer efficient for proliferation-dominated growth. Tumor size is regulated by proliferation speed, oxygen penetration depth and the external pressure [19].

Angiogenesis

As shown in Fig. 2, the tumor-induced angiogenesis is initiated by tumor cells with the shortage of oxygen supply. The cells trigger the release of tumor angiogenic factors (TAF) [7, 18, 20, 21, 34]. Among many tumor growth factors, vascular endothelial growth factor (VEGF) has been identified as one of the key components [7]. VEGF cytokines, released from the tumor cells in hypoxia, diffuse through the extracellular matrix (ECM) - the biological material between tumor and existing vasculature - and produces a chemical gradient. Once VEGF has reached a vessel, it binds to the receptors located on endothelial cells lining blood vessel walls. This stimulates several enzymes (e.g., metalloproteinases) to degrade of basement membrane and sets off a cascade of events which triggers the outgrowth of new vessel sprouts [9, 10, 20]. Endothelial tip cells proliferate and migrate through the ECM. The tip cells follow along the VEGF gradient toward regions of higher concentration (chemotaxis) [21]. As shown in [20, 21], in addition to the soluble isoform of VEGF, the presence of other VEGF isoforms significantly influence morphology of capillary network formation.

After initial sprouts have extended into the ECM for some distance, repeated branching of the tips can be observed. This causes numerous tip-to-sprout transitions. The newly formed vessels may form loops in a process called anastomosis. Along with anastomosis, the formation of lumen establishes a network that allows the blood circulation. The blood starts to circulate in the parts of network with nonzero blood pressure gradient.

There exist many other important factors which both promote and inhibit the process of angiogenesis (e.g., see [9, 10, 15, 20, 21]). Some of them will be discussed in the following sections.

Vascularization

Tumor vascularization is a complex process of vascular network development. It is initiated by the process of angiogenesis and begins with the formation of a primary capillary plexus. Once the sprouts approach the tumor, their branching dramatically increases until the tumor is eventually penetrated by vascular network. Due to better oxygenation, the concentration of TAF decreases also inside the tumor. However, the newly formed vessels are subsequently remodeled by the growing tumor and pushed away producing regions of lesser concentration of oxygen, which initiates TAF production. This stimulates simultaneous growth in size of both tumor and its vasculature [2, 5, 19].

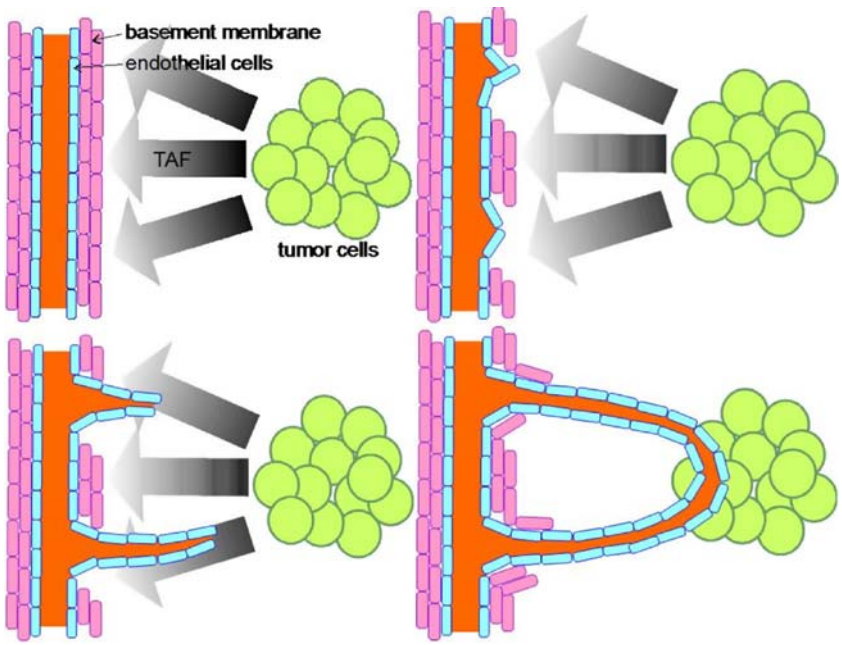

Fig. 2 The scheme of tumor-induced angiogenesis

Tumor vessels can be segregated into three categories [5].

1. Immature - highly proliferative, nonperfused endothelial cell (EC) sprouts emanating from functional vessels.
2. Intermediate - small, perfused vessels which lack support from mural, smooth muscle cells, and pericytes.
3. Mature - larger vessels, which have recruited pericytes, and smooth muscle cells with quiescent ECs and few associated sprouts.

Tumor vessels develop through these stages, beginning with treads of endothelial cells sprouting from functional blood vessels.

Remodeling

The process of tumor vascularization never becomes quiescent because the primitive vessels are continuously remodeled by dynamically evolving angiogenic factors, mechanical forces exerted by growing tumor, blood flow, and intraluminal thrombosis.

Local modifiers of vessel reshapining include growth factors, pericytes, extracellular matrix (ECM), and neighboring cells, such as smooth muscle cells, fibroblasts and macrophages. For example, inhibition of VEGF results in significant increase in EC apoptosis [22] contributing to fast regression of newly formed vessel. The inadequate pericyte coverage is also the reason of vessel decay [5, 22, 23]. As shown in [24, 25], the ECM density and its structure modify the direction of growing vessels. The results shown in [25] confirm different degrees of tumor perfusion or vascularization, depending on the ECM heterogeneity. The vessel wall is not always formed by a homogenous layer of endothelial cells. Instead, it may be lined with neighboring cancer cells and endothelial cells [20] changing vessel functionality.

Global vessel modifiers are: the blood flow and mechanical remodeling involved by the interactions among growing tumor tissue, normal tissue and vasculature. High pressure and shear forces of blood exerted on vessel wall cause its perfusion and dilation. Both the dilated vessels and EC treads without circulating blood collapse. Vessel collapsing in the interior of the tumor initiates percolation process which is driven toward criticality - the percolation threshold - using a mechanism of vessel stabilization by increased blood flow in the remaining vessels [19]. Blood flow is also the source of both shear stress-dependent and pressure-dependent vessels reshaping [26]. However, the most robust remodeling factor is the mechanical interaction between the tumor cells, normal tissue cells and vasculature. The high pressure exerted on the vessel walls can make them collapse. The mechanical forces may change also the location of vessels, destabilizing the tumor growth and changing its direction [4, 19].

Computer models of tumor growth

Mathematical modeling of angiogenesis extends back a number of years [1, 3, 4, 12, 15, 16, 27–29]. The modeling concentrates on key events such as the response of endothelial cells to tumor angiogenic factors secreted by a solid tumor, endothelial cell proliferation, endothelial cell interactions with extracellular matrix macromolecules, capillary sprout branching, blood flow and vessel maturation. The substantial difference with respect to the physical models is that the microscopic state of the cells is defined not only by mechanical variables, such as position, velocity, pressure, but also by internal biological microscopic phenomena reflecting activities of the cells.

A large bibliography about mathematical models of tumor growth driven by the process of angiogenesis can be found in two books edited by Adam and Bellomo [1] and by Preziosi [16] and in more recent overview by Mantzaris *et al*. [15]. Three major categories of models of tumor-induced angiogenesis can be recognize: (a) continuum models that treat the EC and chemical species densities as continuous variables that evolve according to a reaction-diffusion system, (b) mechanochemical models that incorporate some of the mechanical effects of EC-ECM interactions (c) discrete, cellular automata or agent based models in which cells are treated as units which grow and divide according to prescribed rules (d) hybrid multiscale models involving processes from micro-to-macroscale.

Continuum models only incorporate the chemical interactions between the EC and the environment. Among the continuum models, Greenspan proposed some of the earliest mathematical description of tumor growth [30]. His models of avascular tumor growth were formulated as moving boundary problems, in which the solid tumor grows in suspension. The continuum models do not allow for cellular heterogeneity within the tumor mass, and the treatment of the mechanical properties of the tissue is rather simplistic. Moreover, they neglect mechanical interactions between vasculature and its environment. Some types of mechanical interactions were incorporated into mechanochemical models introduced in [30–32]. However, despite continuum models can provide significant insight into the relative role that different process play in the formation of vascular network; they cannot predict its structure. Within these models, it is not possible to capture such important events as repeated sprout branching and the overall dendritic structure of the network.

In contrast to continuum models, many types of discrete techniques have been presented in the literature to explain and describe the branching morphology of the vascular networks. There are, for example, percolation models [33], Eden models [18, 19], random walk and diffusion limited aggregation (DLA) models [24], cell based models [34], lattice models and cellular automata [35–37]. Unlike in the continuum models, discrete models can follow individual cells and can reveal more details about cell dynamics and its interaction with the tissue.

Discrete models are usually hybridized with continuum approaches in which molecular species are represented by their concentration while migrating EC tip cells are mimicked by particles [12, 21, 25]. The Stokes-Lauffenburger [21] model is one of the oldest hybrid models simulating two-dimensional spatial distribution of sprouts. It uses s classic Folkman simulation conditions [6, 7]. The domain is a square (box) of surface S (volume V). The tumor is located at the top center of the domain and the capillary at the bottom. All of the boundaries have no flux conditions for cells and TAF. The evolution of molecular species is governed by reaction-diffusion equations that are discretized on grid. The particle, which dynamics on the TAF concentration field is described by a stochastic differential equation, simulates the migration of EC tip cells. This approach is the source of many other hybrid models (e.g., [12, 17, 18, 24, 25, 35, 37, 38]) which differ in:

1. methodology of simulation of the process of vascularization and tumor growth (stochastic, deterministic, cellular automata, lattice-gas, DLA *etc*.),
2. modeling accuracy and its depth - defined by the number of factors and subprocesses included in the model,
3. assumptions about geometrical properties of the simulation such as: dimensionality (2-D, 3-D), discretization of space and time (on-grid, gridless), structure of vascular network (rigid, structured, unstructured) *etc*.

One of the most popular paradigm used for modeling tumor growth are cellular automata (CA) (see the critical overview [36]). Cellular automata deal with the dynamics of discrete elements populating the nodes of structural (mostly rectangular) grid. The elements take their state from a discrete (finite or infinite) space of states and evolve in discrete space and time. The dynamics of the elements is defined in terms of local, either deterministic or probabilistic, rules. Many models incorporate modifications to the classical definition of a CA hybridizing it, like in the Stokes-Lauffenburger model [21], with continuum fields of diffusive substances, such as nutrients or signaling substances. CA models, however, typically do not address the important mechanical interactions between the tumor and healthy tissue. Complex automata (CxA) are a generalization of cellular automata and represent a scalable hierarchical aggregation of CA and agent-based models [39]. The components represent a sub-system operating on its typical spatial and temporal scales. Globally, CxA can behave either as the classical CA nodes on a structural lattice or as interacting particles whose dynamics is described by the Newtonian laws of motion or stochastic laws. These CxA can be an interesting framework for the development of the multiple scale models.

The accuracy of the computational model is defined by its correspondence to the multiple processes and multiple scales involved in tumor growth (see Fig. 1). Because of the complexity of the entire process, many models to date focus on single key sub-processes, disregarding their interactions with others. Many attempts assume either a static tumor and concentrate on dynamic vascularization in the absence of tumor growth [23–26, 29] or a static network topology [32, 35]. Some of them use dynamic network with blood flowing, neglecting its interaction with concentration fields and tissue components (e.g., [26]).

Multiscale and multi-physics models represent the most advanced simulation methodologies. Multiscale models extend the moving boundary approach to incorporate cellular heterogeneity, intercellular phenomena and the use of more complex mechanical laws to describe the response of the tissue to external forces. Advanced multiscale models of tumor progression are presented in papers by Bellamo *et al*. [1] and by Alacorn *et al*. [17].

The principal weaknesses of these impressive multiscale models are rigid geometric constrains which disable realistic visualization and are the sources of many serious artifacts. The reduction of one spatial dimension belongs to the most drastic simplifications. The 2-D angiogenesis models can adequately approximate only tumors developing on a flat surface. However, even for this case, 2-D approaches result in unrealistic and excessive tumor compartmentalization onto many regions separated by vessels. This compartmentalization may produce the artifact such as the excessive increase of the number of cells in hypoxia in separated regions and, consequently, the increase of microvascular density (MVD). Other 2-D artifact resulting in excessive MVD increase is illustrated in Fig. 3. The 2-D nucleus pushes the vascularization away from its interior, while for 3-D case the tumor cells grow between the vessels.

Other constrains like rigid structure of vascular network (e.g., in [17, 18]), considerably limit the role of vessel remodeling in tumor progression. In [17], for example, the process of angiogenesis is replaced by artificial dilation of blood capillaries, without changes in vessel structure. Moreover, spatial anisotropy imposed by structural CA lattices (rectangular, hexagonal) falsifies both the structural

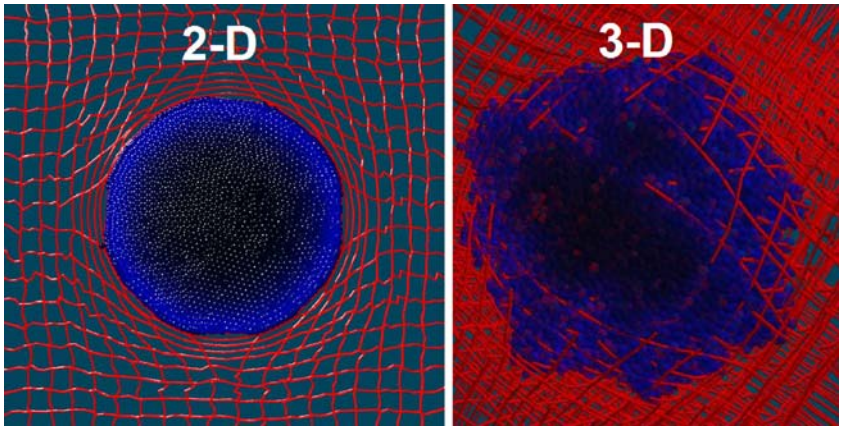

Fig. 3 Two snapshots from simulation of avascular tumor growing in two (2-D) and three (3-D) dimensions in similar conditions. The particle based CxA model was employed. In two dimensions the vasculature is unrealistically stretched and pushed away from the interior of growing nucleus while in 3-D the tumor is rooted by the vessels

characteristic of vascular network and macroscopic behavior of the growing tumor.

Disregarding all microscopic and mesoscopic biological and biophysical processes, in macroscopic scales tumor growth is a purely mechanical phenomenon. Mechanical interactions influences most the structure of vasculature, blood flow, tumor shape and decides about its directional progression. Due to the lack of adequate computational framework any of existing computational paradigms is able to reproduce this basic process. In our opinion, this is the principle obstacle in creation of a truly multiscale model of tumor growth, which not only mimics all the chemical and biochemical inter and intracellular processes but allows for realistic tumor progression in macroscopic scale as well.

Complex automata model driven by particle dynamics

Our complex automata (CxA) model of angiogenesis follows the general principles of particle model described in [40–43]. The system, representing the fragment of tissue, is made of a set $\Lambda_N=\{O_i: O(\mathbf{x}_i,\mathbf{v}_i,\mathbf{a}_i), i=1,...,N\}$ of particles (agents, in terms of CxA terminology [44]), where i is the particle index and N is the number of particles. Each particle is defined by three vectors: position $\mathbf{x}_i$, velocity $\mathbf{v}_i$, and attributes $\mathbf{a}_i$.

The attribute vector $\mathbf{a}=(tp, kd, sz, t_{cell}, t_{hp}, c_{TAF}, c_{O2}, c_{other}, p)$, where:

- tp is particle type: $\in\{$*tumor cell (TC), normal cell (NC), endothelial cell (EC)*$\}$
- kd cell life cycle state: $\in$ $\{$*newly formed, mature, in hypoxia, after hypoxia, apoptosis, necrosis*$\}$
- sz cell size
- t_{cell} cell age (life clock)
- t_{hp} hypoxia time
- c_k concentrations of k=TAF, O2 and other factors
- p total pressure exerted on particle i from its closest neighbors and the walls of the computational box.

In fine-grained models a particle mimics a single cell or components of ECM. Nevertheless, this assumption becomes very computationally demanding for modeling tumors of realistic sizes. The largest molecular dynamics (MD) simulation involved 2×10^{10} particles [45]. However, the number of timestep of this simulation was not so impressive (only 50–100 timesteps). These computational restrictions impose current limits on spatio-temporal scales simulated by our particle model. A tumor of 1 mm in diameter consists at least of a million cells [11]. To simulate the proliferation of a tumor of this size, located in a fragment of tissue of 8 mm^3 in volume in 3-D, one needs at least 1.6×10^7 particles simulated in 10^5 timesteps. This requires approximately the same computational resources as the largest MD simulations.

However, particle method can also be used in its coarse-grained form (as in [42]). In particle models, such as dissipative particle dynamics (DPD) [46], fluid particle dynamics (FPM) [47] or smoothed particle dynamics(SPH) [48], the particle can represent the cluster of atoms or molecules. The clusters interact with each other *via* a central potential such as in the pure MD method. This time, however, the interaction is different than for MD. It usually consists of conservative (repulsive), dissipative and Brownian parts [46, 47]. In a similar way, we can assume that in our coarse-grained model a particle can represent a fragment of tissue with additional attributes, such as concentration of normal, tumor, EC cells and extracellular matrix ingredients. By defining cluster size (the model granulation), this approach allows for simulating tumor growth in various spatio-temporal resolutions.

Unlike in purely fine-grained particle model, where all cells and tissue ingredients are represented by particles, in our model a particle represents a single tumor or normal cell in ECM envelope. Thus, some ECM properties, such as density, can be reflected in parameters of cell-cell interaction model.

In a truly fine-grained model, the vessel walls had to be made of small and thin endothelial cells. Moreover,

sprouting and bifurcation of vessel tip is a very complex biological process involving tens of cells, many growth factors, chemical species and ECM structure [9, 15, 21, 22]. For the sake of simplicity we assume here that the vessel is constructed of tube-like "particles" - EC-tubes - each made of many endothelial cells. As shown in Fig. 4, we define three types of interactions: sphere-sphere (A), sphere-tube (B), and tub-tube (C).

The forces between cells should mimic both mechanical repulsion from squashed cells and attraction due to cell adhesiveness [17] and depletion interactions [43, 49]. The mechanical repulsion can be approximated by Hook law. We assume, for simplicity, that the attractive tail has similar character but it is less rigid than the repulsive part (see Fig. 4D). The attractive forces are short-ranged. This heuristic potential $\Omega(d_{ij})$ (illustrated in Fig. 4D) we define as follows:

$$\Omega(d_{ij}) = \begin{cases} a_1 d_{ij}^2, \text{for } d_{ij} < d_{cut}, \text{where } a = \begin{cases} a_1 \text{ for } d_{ij} < 0 \\ a_2 \text{ for } d_{ij} \geq 0 \end{cases} \\ a_2 d_{cut}^2, \text{for } d_{ij} \geq d_{cut} \end{cases} \quad \text{and } a_1 << a_2 \tag{1}$$

and

$$d_{ij} = \left|\vec{r}_{ij}\right| - \left(r_i + r_j\right) \tag{2}$$

where d_{ij} is the distance between cell walls. In more advanced models, tumor and normal cell interactions can be represented employing different interaction parameters $a_{1,2}$ due to different mechanical properties: elasticity and adherence of normal and tumor cells [15, 17, 39]. The interactions between spherical cells and EC-tubes have similar character. We assume that despite the elongated shape of the tube the interactions are central. The tube-tube interactions are also central. This assumption is justified because torque will not produce remarkable effects for slow and highly dissipative tumor dynamics. Moreover, by neglecting angular momentum, we can reduce computational load required for numerical integration of equations of motion. Only the tips of interacting tubes can fuse them together. Consequently, the chain of tubes forms blood vessels such as in Fig. 4C and in Fig. 8.

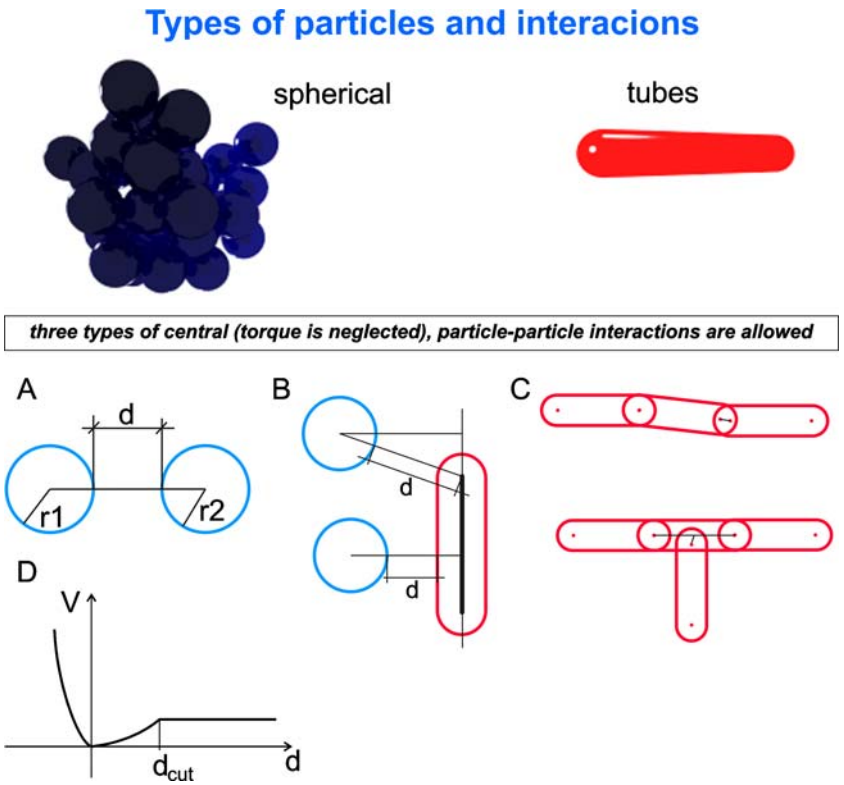

Fig. 4 The types of particles and interactions used in the particle based model

The particle dynamics is governed by the Newtonian laws:

$$m_i \frac{d\mathbf{V}_i}{dt} = -a \cdot \nabla \Omega(d_{ij}) - \lambda \cdot \mathbf{V}_i \qquad \frac{d\mathbf{r}_i}{dt} = \mathbf{V}_i$$
$$r_{ij} = (\mathbf{r}_i - \mathbf{r}_j) \cdot (\mathbf{r}_i - \mathbf{r}_j)^T \tag{3}$$

where m_i, $\mathbf{r}_i$ and $\mathbf{V}_i$ are the mass, position and velocity of particle i, respectively, while λ is a friction coefficient. This set of equations of motion is solved numerically by using direct leap-frog scheme (see overview [43, 49]). The total forces acting on particles are calculated by using linked-cells method combined with the Verlet algorithm (see e.g., in [49, 50]).

The particle system representing a growing tumor is very unstable. The number of cells increases and/or fluctuates because they can replicate or disappear. During the life-cycle, the normal and tumor cells change their states from *new* to *apoptotic* (or *necrotic*) according to their individual clock and oxygen concentration. The cells of certain age and size and being well oxygenated undergo the process of "*mitosis*". They split into two daughter cells. The new formed cell is in *new* state and its diameter is equal to d_{MIN}. The diameter increases with time up to d_{MAX}, proportionally to the oxygen concentration. The minimum and maximum particle diameters depend on the model granularity. Finally, after time T_N, the particles undergo *apoptosis*, i.e., programmed cell death. Consequently, dead cells are removed from the system. For oxygen concentration smaller than a given threshold, the cell (which is not in the *necrotic* state) changes its state to *hypoxia*. Such cells become the source of TAF. The cells, which are in hypoxia for a period of time longer than a given threshold, die and become *necrotic*. We assume that in the beginning, the diameter of a *necrotic* cell decreases twice and, after some time, the cell is removed. This is contrary to apoptotic cells, which are rapidly digested by their neighbors or by macrophages. The diagram of the cell cycle is shown below (Fig. 5). As was mention before, the duration of phases of the cell cycle for normal and tumor cells differs considerably. Also the behavior of tumor and normal cell is different. For example, the proliferation rate of tumor cells, which were in hypoxia state, can change. As shown in Fig. 6, the cells being a certain period of time in hypoxia proliferate faster than those evolving in normal conditions. In Fig. 7 we present two snapshots from simulation of a growing cell cluster.

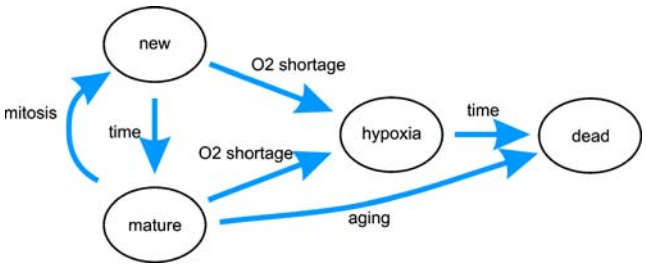

Fig. 5 The simplified diagram of cell fate

The cell cycle for EC-tubes is different than for spherical cells. In fact, EC-tubes are clusters of endothelial cells. The tubes grow both in length and in diameter. The vessels collapse due to a combination of severely reduced blood flow, the lack of VEGF, dilation, perfusion and solid stress exerted by the tumor. However, because the EC-tube is a cluster of EC cells, its division onto two adjoined tubes does not represent the process of mitosis but is a computational metaphor of vessel growth. Unlike, normal and tumor cells, the tubes can appear as tips of newly created capillaries sprouting from existing vessels. The new sprout is formed when the TAF concentration exceeds a given threshold. Then the "vessel particle" undergoes the process of "*mitosis*" directed to the local gradient of TAF concentration. The haptotaxis involving fibronectin [12, 15] is not included yet in the model. In Fig. 8 we show two snapshots from simulation of spontaneously growing tube cluster.

The cells interact with each other not only by means of mechanical forces. As shown in [17], under certain circumstances, cancer cells can modify their environment. Particularly, they are able to increase local acidity. Because tumor cells show greater resistance to acid concentration than the normal cells, they can eliminate normal cells from tumor cells neighborhood by increasing acidity. In our model, totalistic cellular automata rules are used to simulate competition between tissue and tumor cells. The decisions about survival or death of neighboring healthy cells will be taken comparing the intracellular concentration of acid to a critical threshold.

The transport of bloodborn oxygen and TAF into the tissue is modeled by means of reaction-diffusion equations. The distribution of hematocrit is the source of oxygen, while the distribution of tumor cells in hypoxia is the source of TAF. On the other hand, the distribution of cells gives us the spatially distributed sink of both oxygen and TAF. We assume that the cells of any type consume oxygen and the rate of oxygen consumption depends on both cell type and its current state [51]. We assume additionally that only EC-tubes absorb TAF. TAF is washed out from the system due to blood flow. Of course, one could employ more detailed models involving VEGFb absorption in ECM [25], however, at the expense of considerable increase of computational load.

Diffusion of oxygen and TAF is many orders of magnitude faster than the process of tumor growth. On the other hand, the blood circulation is slower than diffusion but still faster than the mitosis cycle (see Fig. 1). Therefore, we can assume that both the concen-

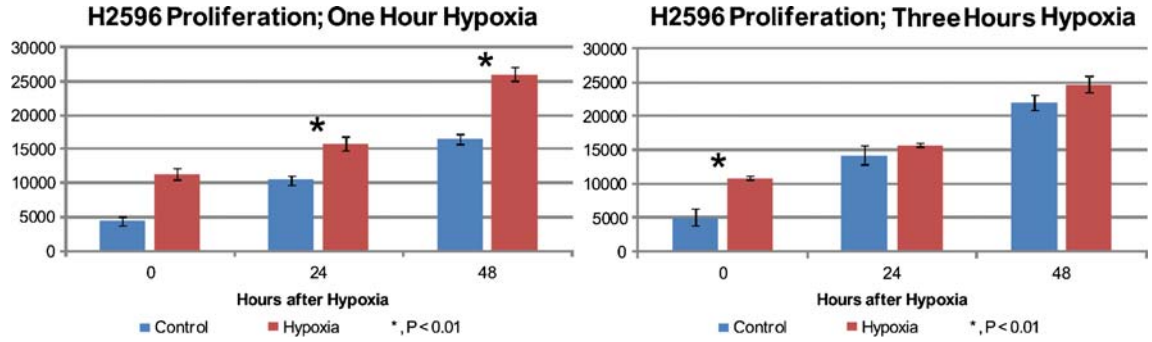

Fig. 6 The diagrams illustrating speed of growth of mesothelioma cell line before (control) and after hypoxia (0, 24 and 48 hours)

trations (of oxygen and TAF) and hydrodynamic quantities are in steady state in the time scale defined by the timestep used for numerical integration of equations of motion (Eq. 3). This allows for employing fast approximation procedures for both calculation of blood flow rates in capillaries and solving the reaction-diffusion equation.

We compute the blood flow rates employing Kirchoff's laws (same as in [17]). We assume that only vessels with circulating blood (anastomosing vessels) are the sources of oxygen. Moreover, both the oxygen and hematocrit concentrations in blood do not change along capillaries and the oxygen supply is proportional to the blood flow rate.

To calculate the concentrations of oxygen and TAF we solve the reaction-diffusion equations numerically by using approximation theory. One can estimate a function f at position $\mathbf{r}$ by using smoothing kernels W as follows:

$$f(\mathbf{r}) = \sum_{j=1}^{n} m_j \frac{f_j}{\rho_j} W(\mathbf{r} - \mathbf{r}_j, h) \tag{4}$$

where m_j is the mass, $\mathbf{r}_j$ is the position, ρ_j is the density and f_j is the quantity f for neighbor particle j, respectively. Here, n is the number of neighboring particles within cut of radius h ($|\mathbf{r} - \mathbf{r}_j| \le h$). When $\mathbf{r}$=$\mathbf{r}_i$, f(r) is denoted by f_i. The smoothing kernel approximates a local neighborhood $\mathbf{r}$ within distance h. Thus, we can estimate the density ρ_i for a particle i at location $\mathbf{r}_i$ by:

$$\rho_i = \sum_{j=1}^{n} m_j W(\mathbf{r}_i - \mathbf{r}_j, h) \tag{5}$$

where j is the index of the neighboring particle. The kernel should be smooth, symmetric and satisfy the following equation:

$$\int_{\Omega} W(\mathbf{r}, h) d\mathbf{r} = 1. \tag{6}$$

We used 3D *poly6* kernel proposed by Muller *et al*. [52].

$$W_{poly6}(\mathbf{r}, h) = \frac{315}{64\pi h^9} \begin{cases} \left(h^2 - |\mathbf{r}|^2\right)^3 & |\mathbf{r}| \le h \\ 0 & \text{otherwise} \end{cases} \tag{7}$$

We selected this kernel due to its simplicity. As shown in [52], better kernels can be used, however, at the cost of computational efficiency. The Laplacian can be approximated then:

$$\Delta f_i = \sum_{j=1}^{n} \frac{m_j}{\rho_j} f_j \cdot \Delta W(\mathbf{r}_i - \mathbf{r}_j, h). \tag{8}$$

Substituting Laplacian in the reaction-diffusion equation by Eq. (8) we got the following expression for concen-

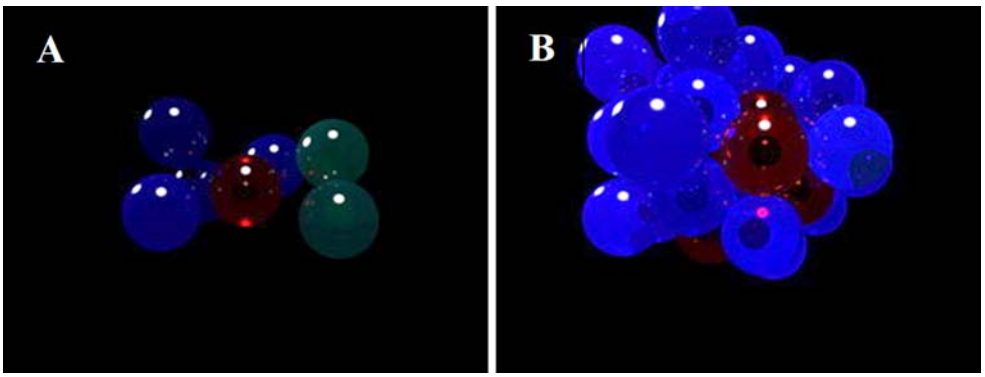

Fig. 7 Two snapshots from simulation of a growing spherical particle cluster due to mitosis of cells

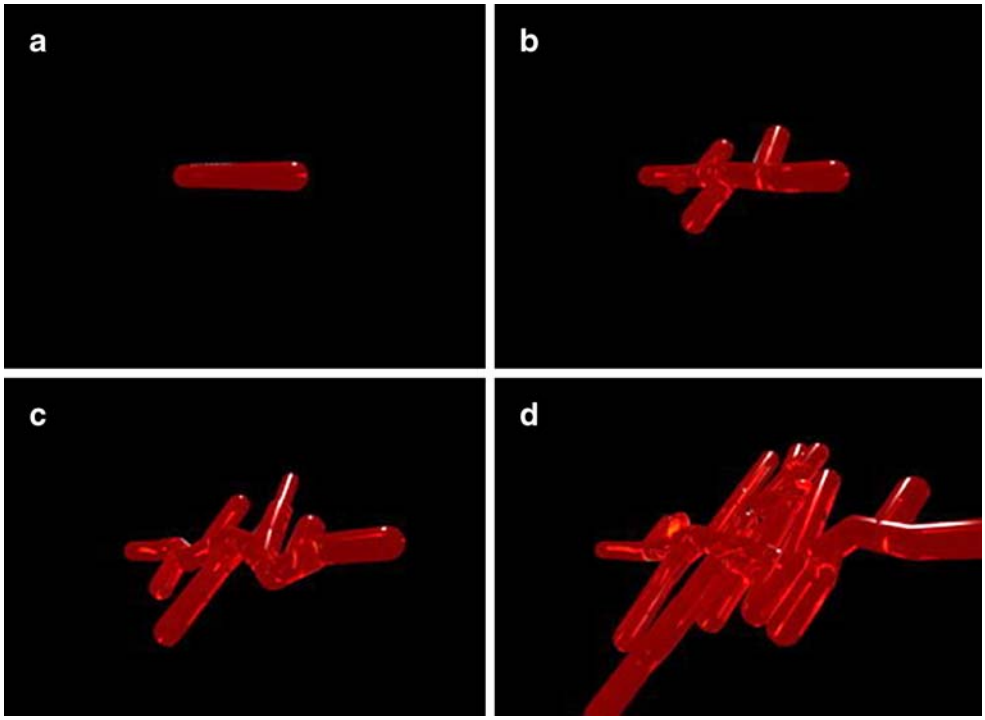

Fig. 8 The snapshots from simulation of growth of tube particle cluster due to mitosis

trations c_i^K of $K=\{oxygen,\ TAF\}$ in particle i (χ^K - reaction factor). When $K=oxygen$, then $I=TAF$ and vice versa.

$$c_i^K = \frac{\left(\frac{\chi_i^I c_i^I}{D} - \sum_{j=1, i\neq j}^{n} \frac{m_j}{\rho_j} c_i^K \cdot \Delta W\left(\mathbf{r}_i - \mathbf{r}_j, h\right)\right)}{\left(\frac{m_i}{\rho_i}\Delta W(0,h) - \frac{\chi_i^K}{D}\right)} \tag{9}$$

By solving this equation iteratively in each time-step of Newtonian equation integration, we obtained the approximate concentration of TAF and oxygen in each particle location.

The particles are confined in the cubical computational box of volume V. Because the average kinetic energy in the system is negligible small, from the virial theorem we obtain that:

$$P \approx \frac{1}{3V} \cdot \sum_{i<j}^{N} \mathbf{F}_{ij} \circ \mathbf{r}_{ij}. \tag{10}$$

The internal pressure increases due to increasing number of particles (cells). The increase of box volume V compensates the pressure increase above a given threshold.

In Fig. 9 we show basic procedures of our CxA particle model, which include the model initialization phase, i.e., definition of initial and boundary conditions, and its evolution driven by the following phenomena, which are modeled explicitly:

a. Newtonian dynamics of interacting cells,
b. diffusion of oxygen and TAF,
c. cellular life cycle modeled by CxA rules,
d. vessels sprouting and growth,
e. vessels remodeling due to flow and maturation.

In the following section, we describe results from modeling of the tumor proliferation in both avascular and vascular phases by using the particle model described above.

Results of modeling

Assumptions and simulation parameters

In this paper we do not investigate a growth pattern of a specific cancer histology. We focus our attention on the functionality and correctness of our model as a metaphor of tumor growth. Below we discuss the parameters and shortcomings we employ in our model.

The spatial scales we used in the particle model are defined by the cell diameter, the size of computational box and microvascular density (MVD). We have assumed that the tumor cell (TC) diameter is 30 μm. It is larger than in typical models (e.g., in [17–19]) (10 μm) but it is smaller than V-79 cell described in [7]. This is a rather technical shortcoming to decrease the computational load. The tumor of about 1 mm in diameter would consists then of 5×10^4

Fig. 9 The main procedures of the model

```
----{1. Initialization}----------------------------------------------------------

define boundary_conditions();
define_initial_conditions();
assign_simulation_parameters();
divide_the_computational_box_onto_sub-boxes();

for each time step:
-----{2. calculate O2 and TAF concentrations in cells and tubes locations}----------
   calculate_diffusion_of _O2();   {Eqs.5,7,9}
   calculate_diffusion_of_TAF();   {Eqs.5,7,9}

------{3. cell dynamics and life-cycle }-----------------------------------------
 for each cell and tube:
    {3.1 mechanical interactions of cells and vessels}.....
     assign_ cells_to_sub-boxes;
     {calculate_cell_interactions_within_sub-boxes_and_their_closest_neighbors for all kind of cells}
     calculate_forces_between_cells; {both tumor and tissue cells}
     calculate_forces_between_tubes;
     calculate_forces_between_tubes_and_cells;
     calculate_new_positions_and_velocities_of_cells {integrate the Newtonian laws of motion}
     calculate_new_positions_and_velocities_of_tubes
     {3.2 cell and vessel life cycle}.....
  change_size(); {the cell diameter is increasing for well oxygenated cells or collapses for cells in
          apoptosis}
  change_state(); {based on age, cell densities, probability of mitosis, apoptosis and necrosis }
          update_time_counters;
                  if conditions are met:
                   proliferate(); {replication, in case of tubes chemotaxis in direction of TAF gradient}
                  if other conditions are met
               quiescent();
          else
                   apoptosis or necrosis(); {rapid size reduction to complete removal in the next steps}
    {3.3 sprouting}.....
  if conditions are met (e.g. TAF concentration>TAFMAX + other factors)
     sprout_out_new_vessels ();
 endfor

-----{4. remodeling}-------------------------------------------------------------
   {4.1 flow}.....
   calculate_blood_flow_intensity_in_vessels():
   calculate_pressure(); {based on pressure in neighboring vessel pipes}
   calculate_flow();   {based on pressure diferences}
   if conditions are met (e.g.VEGF concentration<VEGFMIN || the intensity of flow in the
                  vessel<INTMIN)
    vessel_degradation(); {for immature vessels only}

   {4.2 maturation}.....
    if conditions are met (e.g. time counter>MAXTIME && the intensity of flow in  vessel>INTMAX)
     vessel_maturation();

endfor. W Dzwinel W Dzwinel
```

cells instead of millions. The particles (cells) are confined in the computational box of size 1.5 mm×1.5 mm×1.5 mm (or 2 mm×2 mm×2 mm for the largest simulations). Total number of cells in the box is 10^5 of order. We have assumed that if the total pressure exceeds a given threshold, the stress is dissipated and the pressure in the box stabilizes. In order to keep it constant, those cells which are close to the box walls and which are the most suppressed are removed from the system. The initial state of the particle system at t=0 represents a regularly vascularized region of a given microvascular density MVD with a small tumor in the center (see Fig. 11). Vessels are arranged in a regular grid with a lattice constant a=100 μm. This yields MVD= 100 vessels per mm^2 in 3-D. As shown in Fig. 10, this structure reflects well real oxygenation of modeled tissue fragment.

We have chosen the timestep of simulation assuming typical time scales of cell life cycle and tumor progression rates such as division time, average cell life time in hypoxia, doubling time of tumor volume (see Table 1). In Eden model described in [18, 19] Δt is set to 1 h. Due to cells motion driven by cells proliferation and their death,

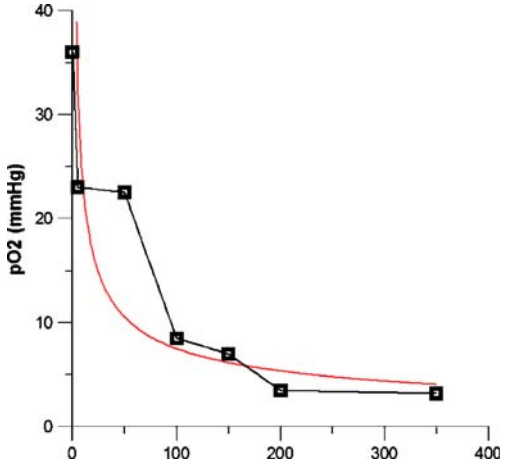

Fig. 10 Oxygen penetration depth for mouse according to [56]. The O_2 pressure (pO_2) dropped exponentially and reached plateau values of 3 mm Hg at around 200 μm away from the blood vessel. Assuming that critical pO_2 for healthy tissue is about 8-10 mmHg while about 2-4 mmHg for tumor cells [51, 54, 56], the average distance to the hypoxic TCs should be about 150 μm. The red curve is the exponential fit of experimental data

the time-step for numerical integration of Eq. (3) in the particle model has to be smaller. On the other hand, because of high dissipation rate in the equations of motion (sufficiently large friction λ in Eq. (3)) the time-step has not to be so rigorously defined as for other particle methods, e.g., such as in molecular dynamics. On the base of our experience we assumed that in our simulations $\Delta t = 0.25$ h.

Functional vessels, i.e., the vessels with flowing blood, are sources of oxygen while the cells are spatially distributed sinks of oxygen. For computational tractability we assumed a fixed O2 secretion rate along the vessel with a given flow intensity. This assumption overestimates the O2 concentration in regions with high MVD, but this does not alter the model outcome significantly [18, 19]. We solve diffusion equation assuming that the diffusion coefficient is $D_{O2}=1.75\times10^{5}$ cm^2/s [51, 53]. The resulting O2 concentration profile is fit to experimental data from Fig. 10. Given this initial configurations, we use Kirchoff's laws to calculate the flow intensities in newly formed anastomoses and remodeled vessels. This then provides us with initial conditions for updating the O2 concentration profiles in the following simulation steps. As shown in Table 1, maximal survival time in hypoxia are considerably lower for normal than for tumor cells, moreover, tumor cells can survive in much lower O2 concentration [39, 54]. The metabolic parameters and thresholds for cells in hypoxia are partly copied from [39, 51, 55] and from experimental results obtained by one of the authors of this paper (A.Z. Dudek). Diffusion coefficient for TAF is assumed to be 10^{-6} cm^2/s [18, 53]. The concentration profiles for TAF and oxygen are updated simultaneously according to Eq. (9).

At the beginning of simulation, apart from the grid of vessels, the box is filled with only normal cells. We assumed that the normal cells do not proliferate and their life-time is very long. However, they can die due to necrotic factors like hypoxia or high local acidity caused by tumor cells [17]. The growing tumor pushes away the vessels, opening the gap of poorly oxygenated cells. When hypoxic region in avascular tumor is sufficiently large to secrete enough quantity of TAF, the angiogenic phase is initiated [6, 10, 54].

The newly formed blood vessels become functional when they form anastomoses allowing for blood flow due to pressure difference on its ends. Otherwise, we assume that the functional capillaries without pericyte support dissolve during 70 h. Moreover, nonfunctional and immature vessels without blood flow are removed from the system after 10 h from the moment the VEGF concentration falls below a given threshold [5, 57]. The values of the most of parameters are copied from existing computational models, e.g., [2, 17–19].

The vessel maturation is controlled by the density of pericytes [5, 15, 22, 23]. The varying degrees of pericyte recruitment indicate differences in the functional status of the tumor vasculature. In our simulations we assume a very simplistic model of vessel maturation. The regression time depends on the local density of EC tubes. If the density is too high regression time is shorter. Dll4 regulates the sprouting rate. The lack of Dll4 results in excessive sprouting of newly formed vessels. As shown in Table 1, some simulation parameters such as those defining particle-particle interactions are specific for our particle model and cannot be measured experimentally. The others, like pressure limits and energy dissipation rates were set heuristically on the base of observation of the model behavior. The majority of measurable biological parameter is typical for similar type of computer modeling presented in [12, 15, 17, 18]. The main parameters are collected in Table 1.

Modeling of avascular phase of tumor growth

Because the size of thecomputational box is about 1.5–2 mm, we assume that the diameter of avascular tumor does not exceed 0.5 mm. It means that the thresholds on vessels sprouting must be kept on such a level that TAF secretion from hypoxic part of the tumor is not sufficient to initiate the process of angiogenesis. The other factor, which controls the tumor growth rate, is the pressure computed from Eq. (10). As shown in Figs. 3; 11, the swelling tumor pushes away the capillaries increasing the space of poorly oxygenated cells in its interior. The nodule after being exposed to the critical stress, gradually relaxes its stress allowing the pathology to continue expanding. At the

Table 1 Main simulation parameters (p.u. – program units)

1. Global physical and numerical parameters			
Name	**Description**	**Values**	**Units**
timestep	The length of timestep	0.25	h
no_timesteps	Typical number of timesteps	10^4 - 10^5	
box_size	The size of computational box	1-2	mm
no_cells	Typical total number of cells simulated	up to 3×10^5	
diffusion_coef_TAF	Diffusion coefficient of TAF	0.002	p.u.*
diffusion_coef_O2	Diffusion coefficient of O2	0.035	p.u.
force_cut_off	Cut-off radius in forces calculations	30	μm
2. Biological and local physical parameters			
a. Tumor cells			
tc_mass	Mass of cell	0.5-1	p.u.
tc_diameter	Diameter of mature cell	15-30	μm
tc_mitosis_rate	Doubling time for tumor	200	h
tc_nutrient_consumption	O2 consumption speed in cell	0.12	p.u./h
tc_nutrient_mitosis	Minimal concentration of O2 for mitosis	6	mmHg
tc_nutrient_hypoxia	Min-Max concentration of O2 in hypoxia	2-5	mmHg
tc_max_hypoxia_time	Maximal life time in hypoxia	50	h
tc_grow_speed	Cell growth rate	0.2	μm /h
tc_min_mitosis_size	Minimal cell size for mitosis	90	%
tc_taf_generation	TAF generation rate	0.1	p.u./h
tc_force_in(out)	Coefficient of cell-cell interactions	0.001	p.u.
tc_mitosis_pressure_limit	Pressure inhibiting cell mitosis	0.3	p.u.
tc_grow_pressure_limit	Pressure inhibiting cell growth	0.5	p.u.
tc_shrink_speed	Speed of necrotic cell shrinking	10	μm /h
tc_dead_age	Maximal time rate of dead cell removal	10	h
tc_dead_reduction	Radius reduction rate for dead cell	1	μm /h
b. healthy cells			
hc_mass	Mass of cell	0.5-1	p.u.
hc_diameter	Diameter of cell	15-30	μm
hc_max_live_age	Maximal life time of cell	5000	h
hc_nutrient_consumption	O2 consumption speed in cell	0.12	$p.u.h^{-1}$
hc_nutrient_mitosis	Minimal concentration of O2 for mitosis	10	mmHg
hc_nutrient_hypoxia	Min-Max concentration of O2 in hypoxia	5-7	mmHg
hc_max_hypoxia_time	Maximal life time in hypoxia	5	h
hc_force_in(out)	Coefficients of cell-cell interactions	0.001	p.u.
hc_shrink_speed	Speed of necrotic cell shrinking	10	μm /h
hc_dead_age	Maximal time rate of dead cell removal	20	h
hc_dead_reduction	Radius reduction rate for dead cell	1	μm /h
c. vessel tubes			
vc_mass	Mass of EC tube	2.3-5	p.u.
vc_diameter	Diameter of EC tube	10-50	μm
vc_ length	The length of the EC tube	70-150	μm
vc_tip_mitosis_rate	Doubling time for vessel tip tubes	200	h
vc_grow_speed	Growth speed	0.2	μm/h
vc_thicken_speed	Thickening speed	0.002	μm/h
vc_min_mitosis_size	Minimal tube diameter for division	95	%
vc_branch_taf_trigger	TAF concentration allowing for sprouting	0.00005	p.u.
vc_force_in(out)	Coefficient of tube-tube interactions	0.001	p.u.
vc_glue_force	Coefficient of forces gluing tubes in vessels	0.005	p.u.
vc_mitosis_pressure_limit	Pressure inhibiting cell mitosis	100	p.u.
vc_grow_pressure_limit	Pressure inhibiting cell growth	100	p.u.
vc_max_flowless_time	Regression time allowed for non-functional vessels	40	h

* p.u. - program units

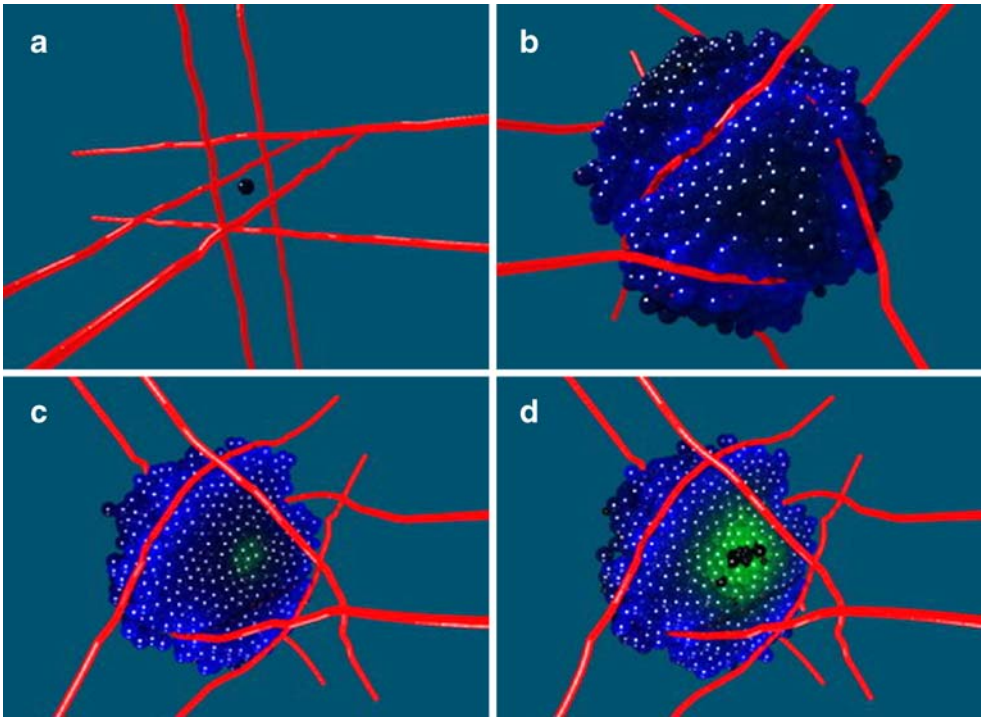

Fig. 11 The snapshots from 3-D simulation of avascular tumor. The tumor from **B** is stable and its size does not increase any longer. **C** and **D** show the cross-sections through the tumor from **B**. The tumor diameter is about 0.35 mm. The initial distance between the vessels is 0.15 mm. Only tumor cells are shown. Blue particles are well oxygenated cells; green particles represent hypoxic cells and black ones the necrotic center. The tissue cells are invisible and we assume that they are well oxygenated

beginning the pressure weakly constrains tumor progression. However, as displayed in Fig. 12, after an initial exponential growth phase leading to tumor expansion, growth saturation is observed even in the presence of a periodically applied nutrient supply. This observation is in a good correspondence with experimental results [7]. The section of the tumor spheroid, shown in Fig. 11, displays a layered structure. A core zone composed mainly of necrotic material is surrounded by a thin layer of quiescent tumor cells and an outer ring of proliferating tumor cells. It is crucial to understand the processes, which are responsible for the growth of a layered and saturating tumor.

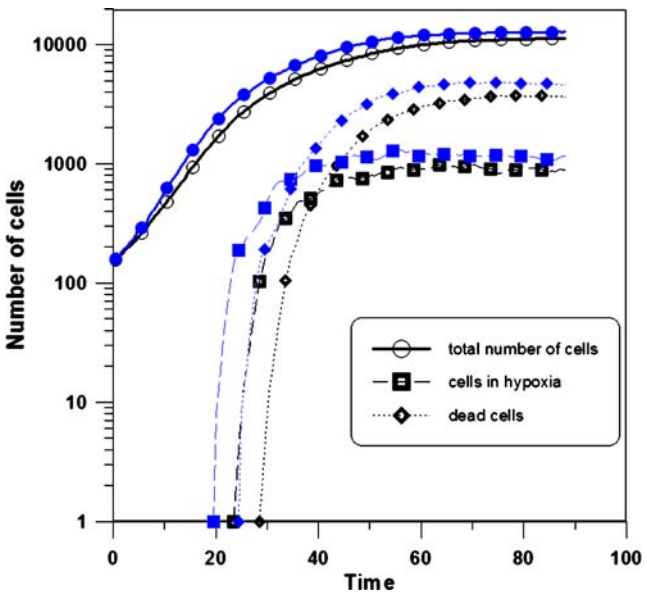

Fig. 12 The plots displaying the number of cells – the total number of tumor cells, cells in hypoxia, and dead cells - with time for growing tumor (see Fig. 11) under different external pressure exerted by the tissue on the tumor mass. The filled symbols correspond to the tumor dynamics inside the tissue which is 10% softer than while open symbols

With increasing size and cell number, the spheroid requires more oxygen (more energy). Since the nutrient concentration is the lowest in the center of the avascular tumor, cells will starve here first, and may eventually die (necrosis). The cells under necrosis swell and burst, forming a necrotic site. The necrotic center collects the necrotic remains, and is much 'softer' than living cell layers [35]. The external pressure stimulates the mixing phenomenon similar in spirit to Rayleigh-Taylor instability boosted additionally by spherical geometry of the particle system (see [41]).

As shown in Fig. 13, the cells from the outer shell are pushed toward the necrotic center. Initially, the inward flow is slow since the necrotic core is not existing or small. Consequently, the outmoving cell population dominates, i. e., the tumor expands. Later on, if the necrotic core has reached a critical size, the inward motion takes over which limits further tumor growth.

The experimental work by Dorie et al. [58] confirms this observation. They showed that there are not only cells moving toward the periphery but also there is a significant number of proliferative and quiescent tumor cells moving from the periphery toward the core area. This inward cell

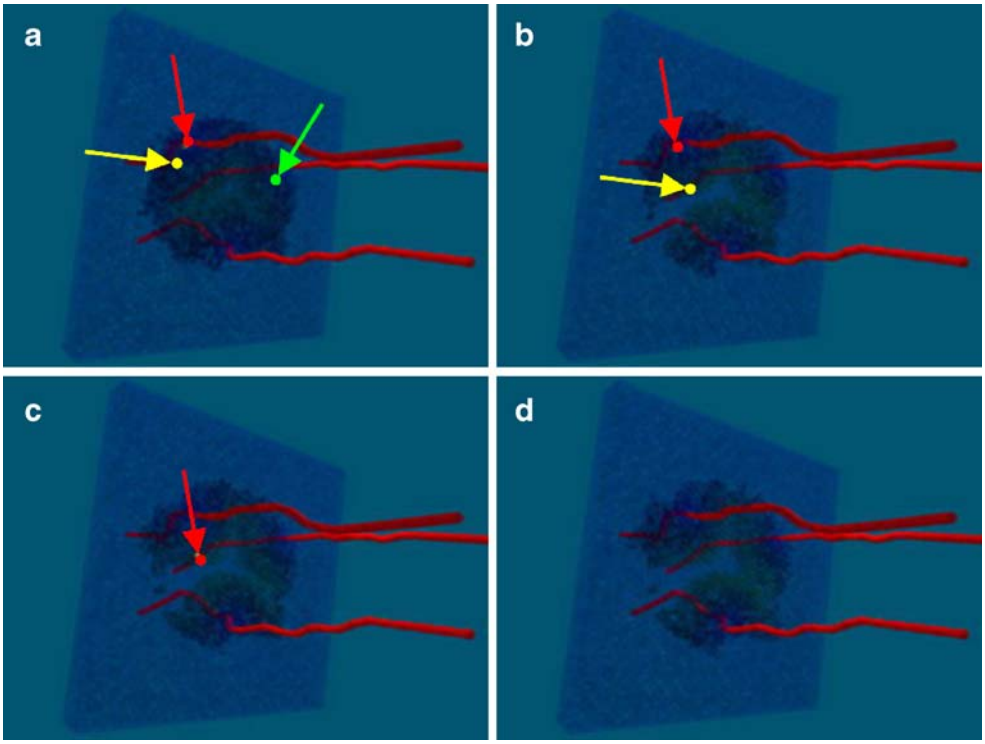

Fig. 13 The snapshots from similar simulation as shown in Fig. 11. The figures illustrate the inward motion of tumor cells from the tumor surface to its necrotic interior. The three arrows of various colors show the cells which disappear, one by one, in the necrotic tumor center

motion is a necessary condition for growth saturation of avascular tumor. If there would be no cell flowing toward the center but only stationary cells and cells moving in the direction of the outer shell, constant oxygen delivery would imply unbounded tumor growth.

This "antagonistic growth direction" was explained in [35] by the chemotaxic migration of tumor cells into the direction of the maximum necrotic signal gradient. Accordingly, in [35] the authors assumed that a diffusible signal emitted by bursting tumor cells is attracting living tumor cells. In our opinion, explanation of the inward cell motion by chemotaxis directed to the necrotic center is superfluous in the context of Occam razor principle.

As shown in Fig. 12, higher external pressure produces tumors of smaller volume. However, this effect is not spectacular. Considerable increase of the external pressure (two times) results in rather small (10%–15%) decrease of tumor volume and causes that also the volume fraction occupied by quiescent cells decreases (by 20% in Fig. 12). Most of solid tumors, even small ones 1–3 mm in diameter, exhibit hypoxic fractions that may range from 10 to 30% [55]. On the other hand, the size of necrotic center cannot shrink to be too small to stop the inward motion of cells.

Its size should be adequate to guarantee the stabilization of the tumor proliferation. We can conclude that high external pressure can decrease the hypoxic fraction of avascular tumor below a threshold required to initiate the angiogenic processes. Such the quiescent tumor can preserve its size for years until the drop of external pressure. It can be caused, e.g., by tissue matrix degradation due to destructive influence of tumor cells (see Fig. 17).

When avascular tumor is getting larger, non-uniform remodeling of capillaries caused by mechanical forces (see Fig. 3B and Fig. 14) may result in hypoxia not only in the central but also in many peripheral parts of the spheroid (see Fig. 14B). Deployment of additional sources of TAF can accelerate the process of angiogenesis. The angiogenesis in the peripheral part of the tumor is even more feasible, because of high density of blood vessels on its border (see Fig. 3 and Fig. 15).

As shown in Fig. 14C, the process of angiogenesis eliminates the hypoxic spots. All the tumor cells are almost uniformly oxygenated. The angiogenic phase stops. In the following section we show how the process of vascularization changes the way of tumor proliferation.

Modeling of tumor vascularization and remodeling

Because of high computational load required for 3-D simulations we assumed that angiogenesis initiates in a very early stage of tumor growth (its diameter is about 100 μm instead of a more realistic 1 mm). This assumption does not change too much the scenario of tumor progression at the start of vascularization process. As shown in Fig. 16, increasing vascularization leads to increasing acceleration growth rate. The tumor evolution starts from power law type of growth. The power order jumps when avascular phase is replaced by angiogenic phase of tumor growth. At this stage however, we cannot estimate which

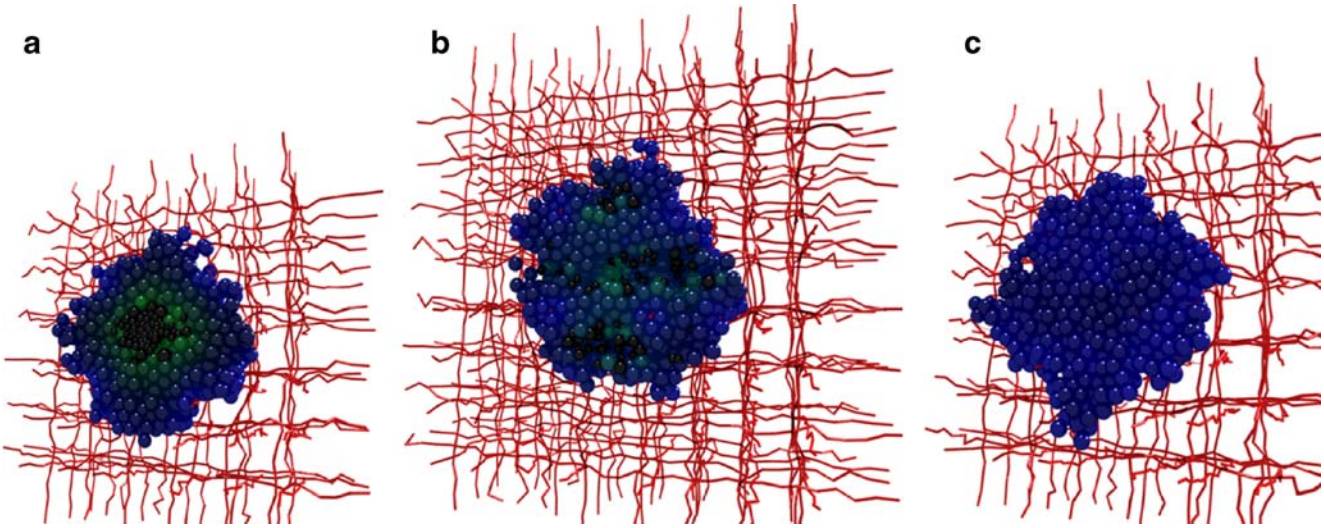

Fig. 14 The cross-sections of avascular tumors (**A**, **B**) and tumor with vascularization (**C**). The tumor diameters are about 0.45 mm (**A**) and 0.55 mm (**B**, **C**). Unlike the tumor from **A**, the tumor from **B** has a few necrotic centers. The tissue cells are invisible and only tumor cells are shown. Blue particles represent well oxygenated cells while green and black cells are hypoxic and necrotic, respectively

kind of growth is expected for a larger tumor. Because of limited size of computational box, the growth is restrained due to increasing pressure.

The tumor evolution in bone cavity is illustrated in Fig. 17. During unrestricted growth (no pressure exerted from healthy tissue) avascular tumor expands fast along the capillary (Fig. 17B). In angiogenic phase, tumor cells fill the whole cavity to the moment when external pressure is higher than the internal pressure. Stimulation of bone lysis by tumor cells allows for local destruction of the porous bone structure. The existing and newly formed blood vessels position themselves within bone matrix niches, helped by high pressure exerted by the tumor on the bone walls (see Fig. 17).

In vascular phase the growing tumor produces its own vascular network with a specific microvascular density (MVD). MVD is used as an important diagnostic tool in cancer therapy [5]. However, MVD is not uniform in tumors. Therefore, a quantitative understanding of the mechanism that causes compartmentalization of the tumor vasculature is critical for more accurate assessment of influence of vascular growth stimulators on tumor proliferation. The mechanism leading to excessive vascularization on the peripheral of the tumor was explained in the previous section (see Figs. 3, 15).

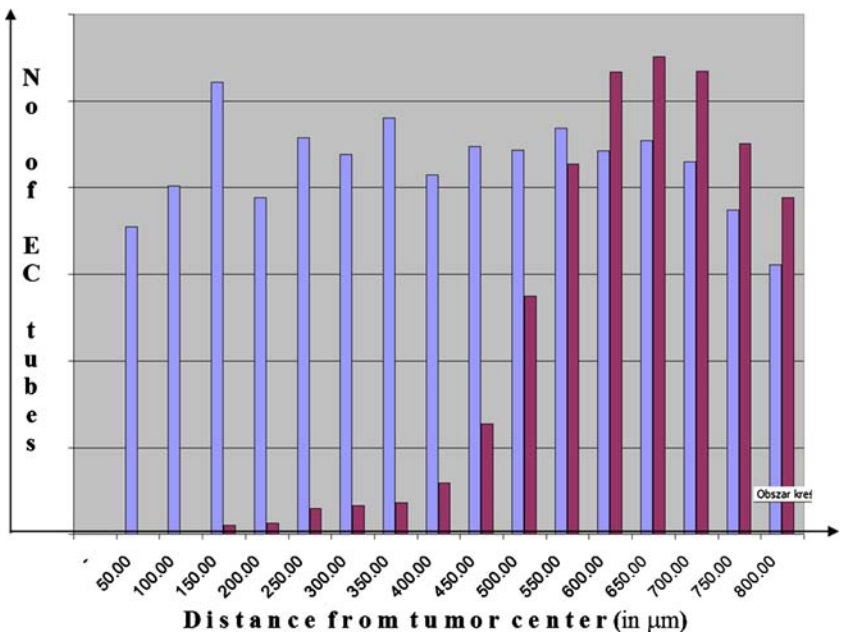

Fig. 15 The histogram of vascularization around the pre-angiogenic tumor. Blue bars show the microvascular density in the absence of tumor

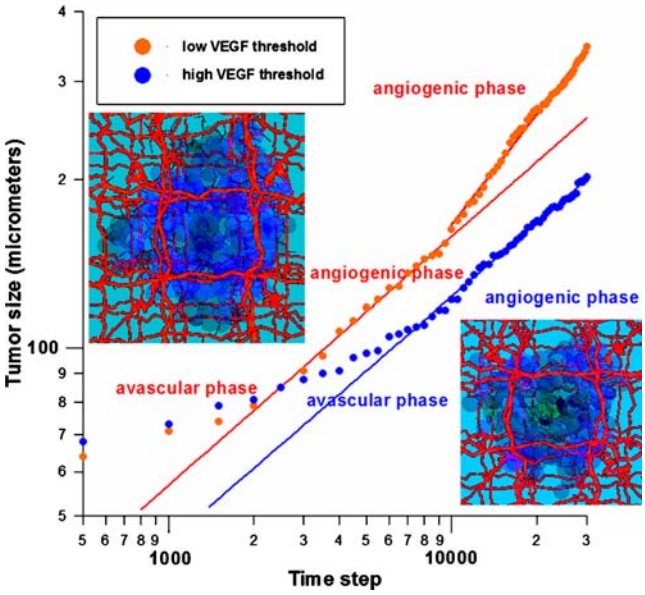

Fig. 16 The acceleration of tumor progression due to angiogenesis assuming two VEGF thresholds

We showed that a high fraction of vessels close to the tumor shell come from normal tissue. These vessels are dense enough to stabilize neovasculature.

The vasculature of tumor interior is in many respects different from the regular vasculature in normal tissues. Tumor vessels are less stable than their normal counterparts and when engulfed by the growing cancerous tissue they undergo processes of regression. As a consequence, newly formed immature vessels fail functionally. Arrested blood flow in deficient blood vessels within tumor interior causes their collapse. This stimulates both the growth of new vessels in this place and increases the blood pressure in other immature vessels. The regression-growth processes repeat all over again. As shown in [18, 19], this process is driven toward criticality - the percolation threshold - *via* a mechanism of vessel stabilization by increase of blood flow in the remaining vessels.

The functional status of the neovasculature depends on many factors. The most unstable are open vessels without blood flowing that dissolve quickly. Only vessels creating anastomozes and pass up blood have a chance to survive. Nevertheless, inhibition of VEGF, e.g., in cocultures, lead to a 75% increase in EC apoptosis [22] which cases vessel regression and blood leaks. All of these factors cause that in most cases the MVD decreases in direction from periphery to the tumor interior [2, 5, 18].

As shown in Fig. 18 which presents the snapshots from 2-D simulation of tumor growth in well oxygenated normal tissue, our particle model reproduces well this highly inhomogeneous tumor specific capillary network. The resulting network is very heterogeneous, composed of dense and void regions, and has distinctly different structure from normal arteriovenous or normal capillary networks [2]. Moreover, the emerging tumor morphology is characterized by the compartmentalization of the tumor into several regions differing in vessel density, and extent of hypoxia [5]. This situation is clearly displayed in Fig. 18.

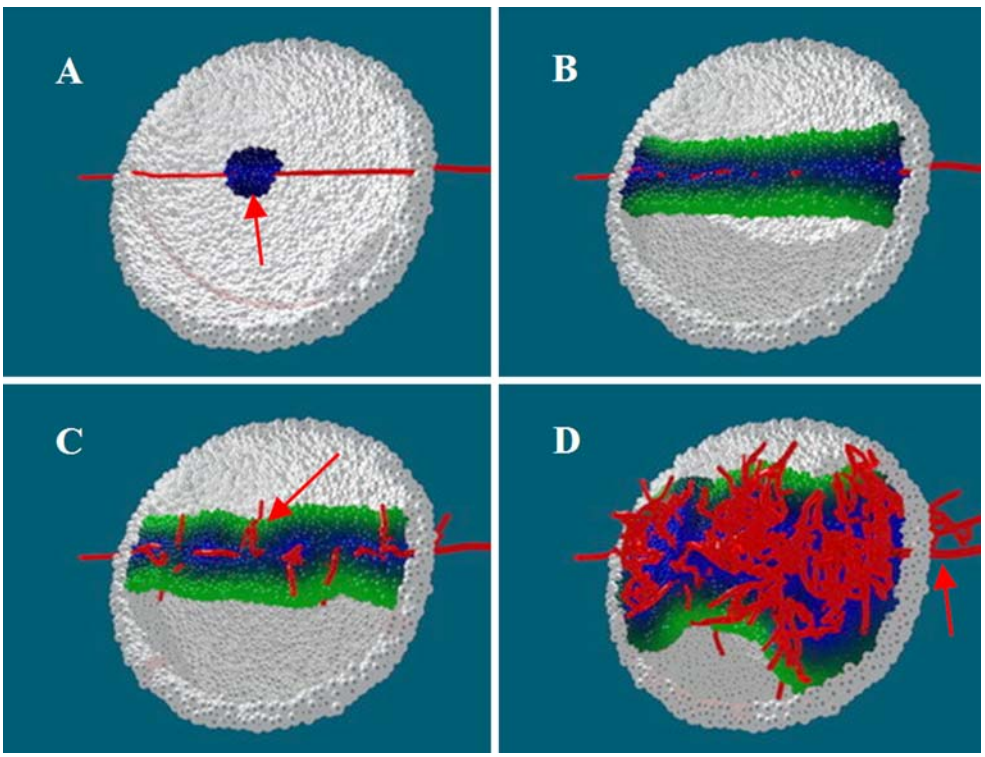

Fig. 17 The cross-section of 3-D tumor evolution in a bone cavity. The white motionless cells represent the bone. The tumor fills the cavity exerting pressure on the bone walls

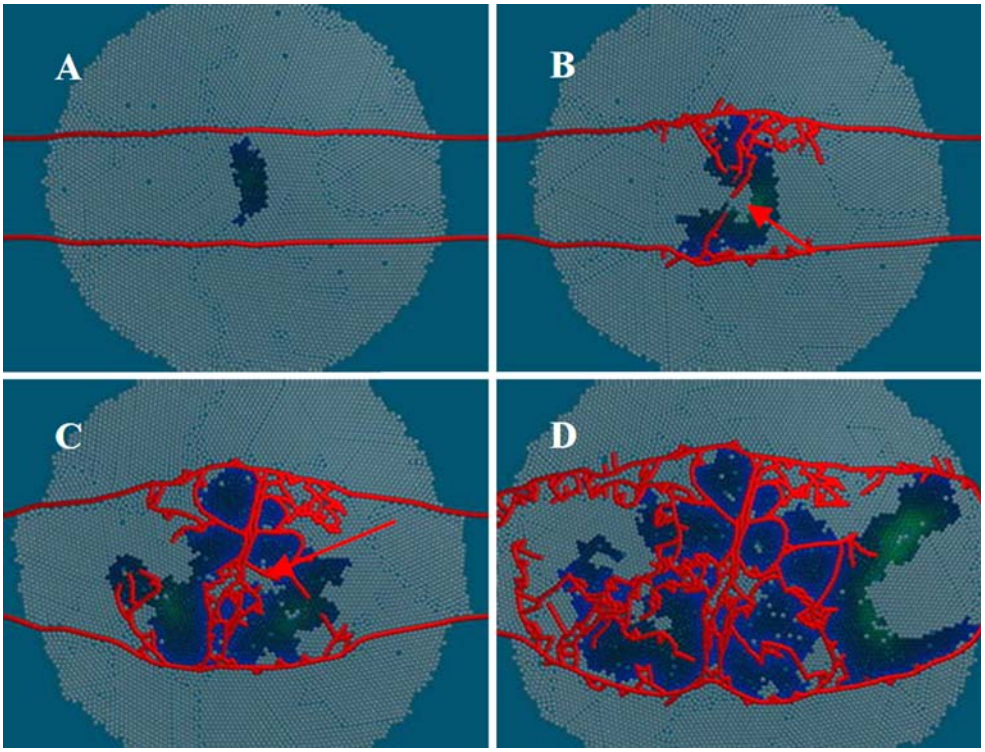

Fig. 18 The snapshots from 2-D simulation of vascularized tumor evolution. The gray cells correspond to normal (healthy) tissue while colored cells represent tumor. The color denotes the extent of cells oxygenation (from blue - highly oxygenated cells, to green – cells in hypoxia). The arrows shows the tissue cells absorbed inside the tumor mass due to mechanical remodeling

In our model we consider two corresponding factors regulating vessels stability. First, we can mimic the activation (inhibition) of delta-like 4 (Dll4)-Notch1 signaling [13, 14]. It regulates the formation of appropriate numbers of tip cells to control vessel sprouting and branching. Inhibition of Notch signaling promotes increased number of tip cells. Conversely, activation of Notch leads to fewer tip cells and vessel branches. Pericytes are the second factor which regulate vessel stability [15, 22, 23]. Pericytes secrete an inhibitor that controls endothelial growth at certain cell densities. The varying degrees of pericyte recruitment indicate differences in the functional status of the tumor vasculature and may reflect varying degrees of maturation of the tumor vascular bed.

Inhibition of Dll4, resulting in excessive sprouting, branching and formation of immature vessels without blood flow, causes that pericytes concentration becomes too low and vessels not supported by pericytes undergo regression. Otherwise, for high activation of Dll4, as in the situation shown in Fig. 19, pericyte covered vessels stabilize and become functional. The maturation of vessels due to pericytes for high activation of (Dll4)-Notch1 signaling were simulated using our 2-D particle model. The snapshots from this simulation are presented in Fig. 20.

Concluding remarks

The concept of complex automata and interacting particles represent a novel framework for constructing multi-scale models of tumor progression. We show that this approach is

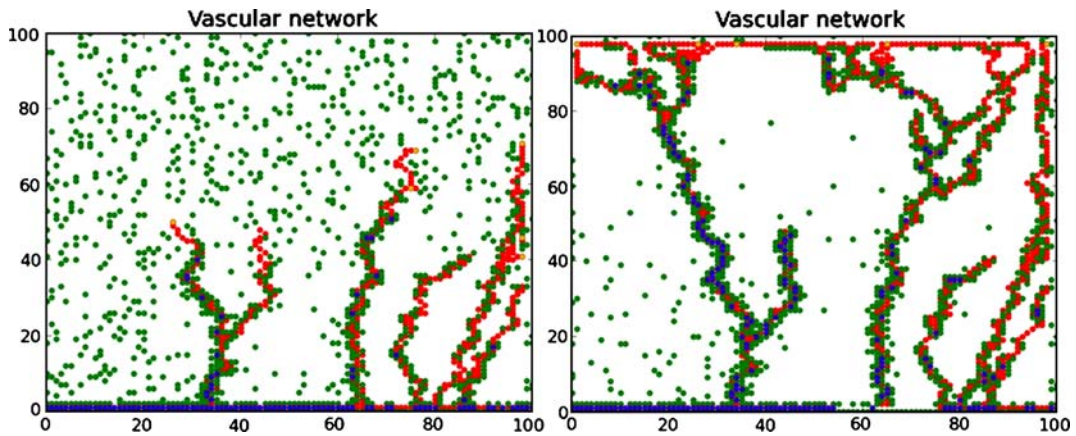

Fig. 19 The snapshot from 2-D model of angiogenesis, showing pericyte uptake by growing vessels

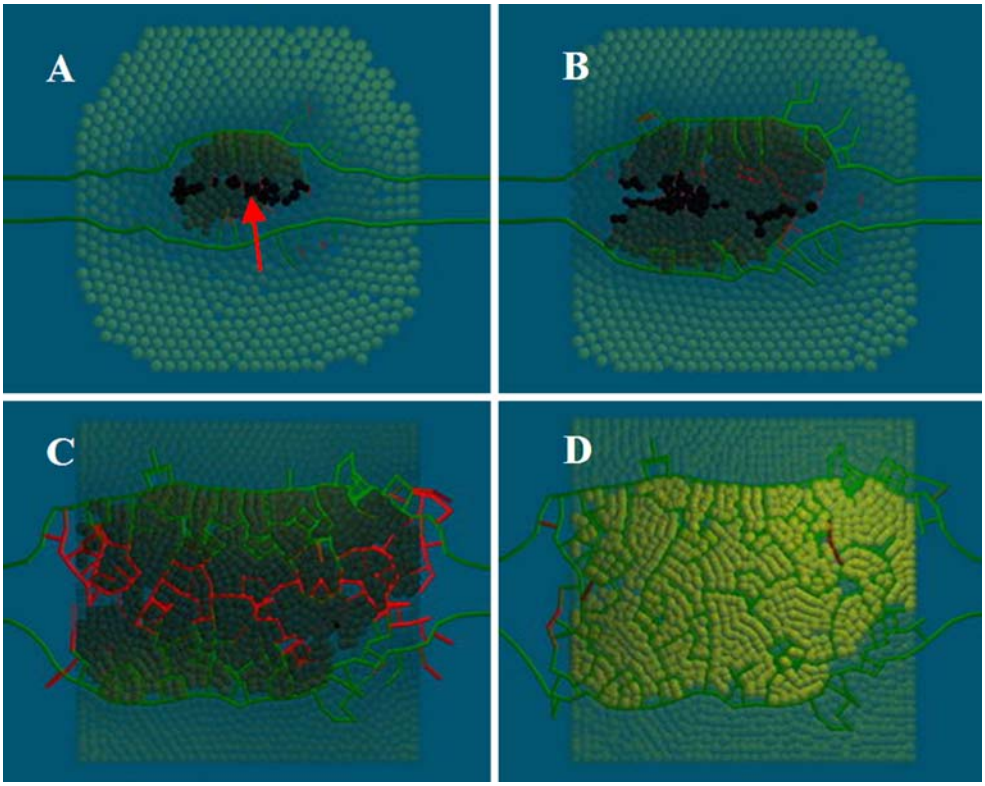

Fig. 20 The snapshots of 2-D simulation of vascularization in tumor. The green vessels represent mature, pericyte covered vessels

competitive both to existing paradigms based on continuum models and classical cellular automata. The possibility of tumor dynamics simulation, which enables mechanical remodeling of the blood vessel system, is the greatest advantage of our model. Moreover, realistic 3-D dynamics of the entire system consisting of the tumor and other tissue cells, blood vessels and blood flow can be reproduced by using the same homogeneous particle model.

Our simulation results indicated that not only redistribution and uptake of angiogenic factors during angiogenesis had significant effects on the structure and functionality of vascular networks. The results of mechanical remodeling can suggest as follows.

1. The layered structure of tumor can be explained solely by the self-organized growth of an initially small number of tumor cells.
2. The inward motion of peripheral tumor cells to its necrotic interior can be explained on purely mechanical ground, without somewhat suspicious necrotic chemotaxis suggested in [35].
3. Larger value of MVD on the tumor peripheral is initiated due to mechanical interaction of expanding tumor borders on existing vasculature.
4. External pressure decelerates tumor proliferation. It evolves to a quiescent state.
5. Our modeling results support controversy to Folkman's optimistic declaration that disruption of angiogenesis yields a starving tumor, which eventually dies. As show the results produced by our model, due to mechanical remodeling of healthy tissue, many disparate fragments of tumor become very well oxygenated. Expanding tumor can push out healthy cells and use regular vasculature to support its growth without the need of excessive angiogenesis.
6. The functionality of neovasculature depends on the balance between pericyte and Dll4 concentrations.

To check if the vascular networks generated in numerical simulations are really similar to the realistic ones we plan to validate our model. This validation will be conducted on the basis of the comparison between realistic images of tumor vascular networks from confocal microscopy and computer experiments. The comparisons will be made employing structural properties of tumor vascularization. The vascular networks can be described by the feature vectors with statistical and/or algebraic descriptors of complex networks [59] as the feature vector components. Finally, pattern recognition methods such as clustering and feature extraction will be used for the vector classification.

The computational complexity and modeling constraints are the main disadvantages of our model. The first problem results from shortcomings we used in our simulations. We applied our particle model to a more developed stage of tumor growth, where the tumor is likely to comprise millions of cells rather than thousands of cells. To solve this problem we need to define a multi-scale model and resort to parallel computing techniques. Although this

certainly implies some degree of complication from the computational point of view, the particle model is not too difficult to implement in parallel [43, 49, 60]. The most serious modeling constraints and simplifications used in our model are as follows:

1. Due to limited size of computational box and growing number of cells the pressure in the box increases. Computationally expensive procedures have to be used to maintain constant pressure inside the box.
2. The cells interaction is radial, which suggests that they are of spherical shape. Implementation of more realistic anisotropic interactions is very demanding computationally.
3. We use for simplicity rigid EC-tubes instead of EC cells, which influences the shape of vessels and may introduce structural artifacts.

Our model of tumor-induced angiogenesis addresses a limited number of biological processes. For example, blood hydrodynamics have received much less attention than in other models (e.g., in [3, 4, 17, 18, 29]). We did this intentionally to reduce the computational load. However, we definitely agree that in larger tumors, vascular remodeling due to blood circulation cannot be neglected. The existing flow models (e.g., as in [17, 18]) can be easily adapted in the scope of our particle model. For simplicity, we neglect also other phenomena. In particular, our model has not addressed the effect of perfusion and different concentration of oxygen along the vessel. Moreover, we consider only oxygen as the nutrient while tumor cells often do not require much oxygen for growth, but glucose, fat, and amino acids. Another area in which our model could be improved is introduction of microscopic sub-models representing important intra cellular phenomena such as cell proliferation in hypoxic conditions. This challenge, however, can be undertaken provided that the efficient parallel version of the model will be implemented.

In our CxA framework it is easy both to develop principal mechanisms of tumor dynamics such as cell proliferation, vascularization, vessels remodeling and incorporate sub-models of other important processes such as microscopic intracellular phenomena, blood circulation, and extracellular matrix models. The particle model can be supplemented by more precise models of reproduction mechanism, cell-life cycle, lumen growth dynamics, haptotaxis mechanism and others. Some models of intracellular phenomena can be copied directly from the work of Alancorn *et al*. [17]. Moreover, more angiogenic factors can be considered, such as various TAF activators and inhibitors. Instead of a simplistic model of blood circulation, advanced blood flow algorithms from Chaplain [12] and Stephanou *et al*., [4, 29] can be implemented in a straightforward way.

For simplicity, our model does not reflect the influence of the extracellular matrix composition on endothelial cell migration and network formation [15]. These very important processes can be simulated easily employing more complicated (e.g., anisotropic) interaction forces between cells. One can assume, for example, that the particle represent the cell with a fragment of extracellular matrix. We can then use interaction forces depending on both the range and the angle of interactions. A more realistic though more computationally demanding way for simulating processes occurring in ECM involves additional type of particles representing various ECM components.

Most of these possible improvements will require supercomputing power to simulate realistic tumor sizes. This is mainly due to the assumption we made that one particle corresponds to a single cell. This puts the upper limit on the size of simulated 3-D system to a few millimeters or at most centimeters when employing nowadays high performance multiprocessor systems. However, as shown in [42, 43, 49], particle models can be used for simulating fluid flows in various spatio-temporal scales by using a coarse graining procedure. We postulate that a similar procedure can be defined for modeling the tissue. Depending on the spatio-temporal scale of simulation, the particle can represent a cell, a cell with a fragment of ECM matrix, cluster of cells and fragments of ECM matrix, or a cloud made of mixture of cells, fragments of ECM matrix and microscopic blood capillaries. If such scalability of the particle model is possible, this would allow for simulating tumors in various spatio-temporal scales from small avascular clusters to large masses.

In summary, we showed that the CxA particle model developed in this study can be used as a robust modeling framework for developing more advanced tumor growth models. Consequently, these models can be used to evaluate the effects of various types of therapies on tumor dynamics, understanding interactions between various growth factors, and to generate experimentally testable hypotheses.

Acknowledgments This research is financed by the Polish Ministry of Education and Science, Project No.3 T11F 010 30, internal AGH Institute of Computer Science grant and Vlab project of National Science Foundation. The exemplar movies from simulations can be downloaded from http://www.icsr.agh.edu.pl/~wcislo/Angiogeneza/index.html.

References

1. Bellomo N, de Angelis E, Preziosi L (2003) Multiscale modeling and mathematical problems related to tumor evolution and medical therapy. J Theor Med 5:111–136
2. Gee MS, Procopio WN, Makonnen S, Feldman MD, Yeilding NM, Lee WF (2003) Tumor vessel development and maturation

impose limits on the effectiveness of anti-vascular therapy. Am J Pathol 162:183–193
3. McDougall SR, Anderson ARA, Chaplain MAJ, Sherratt JA (2002) Mathematical modelling of flow through vascular networks: implications for tumour-induced angiogenesis and chemotherapy strategies. Bull Math Biol 64:673–702
4. Stéphanou A, McDougall SR, Anderson ARA, Chaplain MAJ, Sherratt JA (2005) Mathematical modelling of flow in 2D and 3D vascular networks: Applications to anti-angiogenic and chemotherapeutic drug strategies. J Math Comput Model 41:1137–1156
5. Eberhard A, Kahlert S, Goede V, Hemmerlein B, Plate KH, Augustin HG (2000) Heterogeneity of angiogenesis and blood vessel maturation in human tumors: Implications for antiangiogenic tumor therapies. Cancer Res 60:1388–1393
6. Folkman J (1971) Tumor angiogenesis: Therapeutic implications. N Engl J Med 285:1182–1186
7. Folkman J, Hochberg M (1973) Self-regulation of growth in three dimensions. J Exp Med 138:745–753
8. Folkman J, Hochberg M (1973) Self-regulation of growth in three dimensions. J Exp Med 138:745–753
9. Ferrara N, Chen H, Smyth DT, Gerber HP, Nguyen TN, Peers D, Chisholm V, Hillan KJ, Schwall RH (1998) Vascular endothelial growth factor is essential for corpus luteum angiogenesis. Nat Med 4:336–340
10. Folkman J (2003) Angiogenesis and apoptosis. Semin Cancer Biol 13:159–167
11. Asosingh K, de Raeve H, Menu E, van Riet I, van Marck E, van Camp B, Vanderkerken K (2004) Angiogenic switch during 5T2MM murine myeloma tumorigenesis: Role of CD45 heterogeneity. Blood 103:3131–3137
12. Chaplain MAJ (2000) Mathematical modelling of angiogenesis. J Neuro-Oncol 50:37–51
13. Hellstrom M, Phng L-K, Hofmann JJ, Wallgard E, Coultas L, Lindblom P, Alva J, Nilsson A-K, Karlsson L, Gaiano N, Yoon K, Rossant J, Iruela-Arispe M-L, Kale´n M, Gerhardt H, Betsholtz CH (2007) Dll4 signaling through Notch1 regulates formation of tip cells during angiogenesis. Nature 445:422–425
14. Nogueratroise I, Daly Ch, Papadopoulos NJ, Coetzee S, Boland P, Gale NW, Lin HC, Yancopoulos GD, Thurston G (2006) Blockade of Dll4 inhibits tumour growth by promoting non-productive angiogenesis. Nature 444:1032–1037
15. Mantzaris N, Webb S, Othmer HG (2004) Mathematical Modeling of Tumor-induced Angiogenesis. J Math Biol 49: 1432–1416
16. Preziozi L (ed) (2003) Cancer modelling and simulation. Chapman & Hall/ CRC Mathematical Biology & Medicine 426
17. Alarcon T, Byrne H, Maini PK (2005) A multiple scale model for tumor growth. Multiscale Model Simul 3:440–475
18. Lee D-S, Rieger H, Bartha K (2006) Flow correlated percolation during vascular remodeling in growing tumors. Phys Rev Let 96:058104–1-4
19. Rieger H, Bartha K (2006) Vascular network remodeling via vessel cooption, regression and growth in tumors. J Theor Biol 241:903–918
20. Carmeliet P, Jain RK (2000) Angiogenesis in cancer and other diseases. Nature 407:249–257
21. Stokes CL, Lauffenburger DA (1991) Analysis of the roles of microvessel endothelial cell random motility and chemotaxis in angiogenesis. J Theor Biol 152:377–403
22. Darland DC, Massingham LJ, Smith SR, Piek E, Saint-Geniez M, D'Amore PA (2003) Pericyte production of cell-associated VEGF is differentiation-dependent and is associated with endothelial survival. Dev Biol 264:275–288
23. Nehls V, Denzer K, Drenckhahn D (1992) Pericyte involvement in capillary sprouting during angiogenesis in situ. Cell Tissue Res 270:469–474
24. Amyot F, Small A, Gandjbakhche AH (2006) Stochastic modeling of tumor induced angiogenesis in a heterogeneous medium, the extracellular matrix. In: Proc 28th IEEE EMBS Annual International Conference New York City, USA, 30 Aug- 3 Sept 2006
25. Milde F, Bergdorf M, Koumoutsakos PA (2008) Hybrid model of sprouting angiogenesis. Lect Notes Comp Sci 5102:167–176
26. Godde R, Kurz H (2001) Structural and biophysical simulation of angiogenesis and vascular remodeling. Dev Dyn 220:387–401
27. De Angelis E, Preziosi L (2000) Advection-diffusion models for solid tumour evolution in vivo and related free boundary problem. Math Mod Meth Appl Sci 10:379–407
28. Stein AM, Demuth T, Mobley D, Berens M, Sander LMA (2007) Mathematical model of glioblastoma tumor spheroid invasion in a three-dimensional in vitro experiment. Biophys J 92:356–365
29. Stéphanou A, McDougall SR, Anderson ARA, Chaplain MAJ (2006) Mathematical modelling of the influence of blood rheological properties upon adaptative tumour-induced angiogenesis. Math Comput Model 44:96–123
30. Greenspan HP (1976) On the growth and stability of cell cultures and solid tumours. J Theor Biol 56:229–242
31. Luo S, Nie Y (2004) FEM-based simulation of tumor growth in medical image. Medical Imaging 2004:Visualization, Image Guided Procedures, and Display. In: Galloway RL (ed) Proceedings of SPIE 5367:600-608
32. Szczerba D, Lloyd BA, Bajka M, Szekely GA (2008) Multi-physics model of Myoma growth. Lect Notes Comput Sci 5102:187–196
33. Cavalcante FSA, Moreira AA, Costa UMS, Andrade JS Jr (2002) Self-organized percolation growth in regular and disordered lattices. Stat Mech Appl Phys A 311:313–319
34. Bauer AL, Jackson TL, Jiang YA (2007) Cell-based model exhibiting branching and anastomosis during tumor-induced angiogenesis. Biophys J 92:3105–3121
35. Dormann S, Deutsch A (2002) Modeling of self-organized avascular tumor growth with a hybrid cellular automaton. In Silico Biol 2:393–406
36. Moreira J, Deutsch A (2002) Cellular automaton models of tumor development: A critical review. Adv Complex Syst 5:247–269
37. Topa P (2008) Dynamically reorganising vascular networks modelled using cellular automata approach. Lect Notes Comput Sci LNCS 5191:494–499
38. Wcisło R, Dzwinel W (2008) Particle based model of tumor progression stimulated by the process of angiogenesis. Lect Notes Comput Sci ICCS 2008 LNCS 5102:177–186
39. Hockel M, Vaupel P (2001) Tumor hypoxia: Definitions and current clinical, biologic, and molecular aspects. J Natl Cancer Inst 93:266–276
40. Dzwinel W, Alda W, Yuen DA (1999) Cross-scale numerical simulations using discrete-particle models. Mol Simul 22:397–418
41. Dzwinel W, Alda W, Pogoda M, Yuen DA (2000) Turbulent mixing in the microscale. Phys D 137:157–171
42. Dzwinel W, Boryczko K, Yuen DA (2003) A discrete-particle model of blood dynamics in capillary vessels. J Colloid Int Sci 258:163–173
43. Dzwinel W, Yuen DA, Boryczko K (2006) Bridging diverse physical scales with the discrete-particle paradigm in modeling colloidal dynamics with mesoscopic features. Chem Eng Sci 61:2169–2185

44. Hoekstra AG, Lorenz E, Falcone LC, Chopard B (2007) Towards a complex automata framework for multi-scale modeling: Formalism and the scale separation map. Lect Notes Comput Sci 4487:1611–3349
45. Kadau K, Germann TC, Lomdahl PS (2004) Large-scale molecular-dynamics simulation of 19 billion particles. Int J Mod Phys C 15:193–201
46. Hoogerbrugge PJ, Koelman JMVA (1992) Simulating microscopic hydrodynamic phenomena with dissipative particle dynamics. Europhys Let 19:155–160
47. Español P (1998) Fluid particle model. Phys Rev E 57:2930–2948
48. Monaghan JJ (1992) Smoothed particle hydrodynamics. Annu Rev Astronomy Astrophys 30:543–574
49. Dzwinel W, Boryczko K, Yuen DA (2006) Modeling Mesoscopic Fluids with Discrete-Particles. Methods, Algorithms and Results. In: Spasic AM, Hsu JP (eds) Finely Dispersed Particles: Micro-, Nano-, and Atto-Engineering. Taylor&Francis, CRC Press, pp 715-778
50. Haile PM (1992) Molecular Dynamics Simulation. Wiley&Sons, New York
51. Vaupel P, Kallinowski F, Okunieff P (1989) Blood Flow, Oxygen and Nutrient Supply, and Metabolic Microenvironment of Human Tumors: A Review. Cancer Res 49:6449–6465
52. Muller M, Charypar D, Gross M (2003) Particle-Based Fluid Simulation for Interactive Applications. In: Proceedings of Eurographics/SIGGRAPH Symposium on Computer Animation. San Diego 27-31 July 2003:154-372
53. Grote J, Suskind R, Vaupel P (1977) Oxygen diffusivity in tumor tissue (DS-Carcinosarcoma) under temperature conditions within the range of 20–40C. Pflugers Arch 372:37–42
54. Maxwell PH, Ratcliff PJ (2002) Oxygen sensors and angiogenesis. Semin Cell Dev Biol 13:29–37
55. Moulder JE, Rockwell S (1984) Hypoxic fractions of solid tumors: experimental techniques, methods of analysis, and a survey of existing data. Int J Radiat Oncol Biol Phys 10:695–712
56. Filho IPT, Leunigt M, Yuant F, Intaglietta M, Jaint RK (1994) Noninvasive measurement of microvascular and interstitial oxygen profiles in a human tumor in SCID mice. Proc Nad Acad Sci USA 91:2081–2085
57. Gridley T (2007) Vessel guidance. Nature 445:722–723
58. Dorie MJ, Kallman RF, Rapacchietta DF, Van Antwerp D, Huang YR (1982) Migration and internalization of cells and polystyrene microsphere in tumor cell spheroids. Exp Cell Res 141:201–209
59. Newman MEJ (2003) The structure and function of complex networks. SIAM Review 45:167–256
60. Boryczko K, Dzwinel W, Yuen DA (2002) Parallel implementation of the fluid particle model for simulating complex fluids in the mesoscale. Concurrency and Computation: Practice and Experience 14:1–25